ELSEVIER

Neurobiology of Aging 33 (2012) 2172–2185

NEUROBIOLOGY OF AGING

www.elsevier.com/locate/neuaging

Effect of melatonin on α-synuclein self-assembly and cytotoxicity

Kenjiro Ono[a], Hideki Mochizuki[b], Tokuhei Ikeda[a], Tomoko Nihira[c], Jun-ichi Takasaki[a], David B. Teplow[d], Masahito Yamada[a,*]

[a] *Department of Neurology and Neurobiology and Aging, Kanazawa University Graduate School of Medical Science, Kanazawa, Japan*
[b] *Department of Neurology, Osaka University Graduate School of Medicine, Osaka, Japan*
[c] *Department of Neuro-Regenerative Medicine, Kitasato University, Sagamihara, Japan*
[d] *Department of Neurology, David Geffen School of Medicine, and Molecular Biology Institute and Brain Research Institute, University of California, Los Angeles, CA, USA*

Received 24 March 2011; received in revised form 1 October 2011; accepted 15 October 2011

Abstract

α-Synuclein (αS) assembly has been implicated as a critical step in the development of Lewy body diseases such as Parkinson's disease and dementia with Lewy bodies. Melatonin (Mel), a secretory product of the pineal gland, is known to have beneficial effects such as an antioxidant function and neuroprotection. To elucidate whether Mel has an antiassembly effect, here we used circular dichroism spectroscopy, photoinduced crosslinking of unmodified proteins, thioflavin S fluorescence, size exclusion chromatography, electron microscopy and atomic force microscopy to examine the effects of Mel on the αS assembly. We also examined the effects of Mel on αS-induced cytotoxicity by assaying 3-[4,5-dimethylthiazol-2-yl]-2,5-diphenyltetrazolium bromide metabolism in αS-treated, primary neuronal cells. Initial studies revealed that Mel blocked αS fibril formation as well as destabilizing preformed αS fibrils. Subsequent evaluation of the assembly-stage specificity of the effect showed that Mel was able to inhibit protofibril formation, oligomerization, and secondary structure transitions. Importantly, Mel decreased αS-induced cytotoxicity. These data suggest a mechanism of action for Mel, inhibition of assembly of toxic polymers and protection of neurons from their effect.

Keywords: Parkinson's disease; Dementia with Lewy bodies; α-synuclein; Melatonin; Oligomers; Cytotoxicity

1. Introduction

Parkinson's disease (PD) is 1 of the most common neurodegenerative diseases affecting mainly the extrapyramidal motor system (Forno, 1996). The major lesion in PD resides in the dopaminergic neurons in the substantia nigra, as well as other brain stem nuclei including locus coeruleus and dorsal motor vagal nucleus with appearance of Lewy bodies (LBs) (Forno, 1996). Dementia with LBs (DLB) is a progressive dementing disorder of the elderly clinically characterized by fluctuation in mental decline, visual hallucinations, parkinsonism, and widespread distribution of LBs in the brain (McKeith et al., 2005). LBs constitute the main histopathological features of PD and DLB, and are comprised of amyloid-like fibrils composed of a small protein (approximately 14 kDa) named α-synuclein (αS) (Baba et al., 1998; Forno, 1996; Goedert, 2001). Several transgenic animal models overexpressing human αS display varying degrees of biochemical, pathological, and clinical abnormalities reminiscent of PD (Feany and Bender, 2000; Giasson et al., 2002; Lee et al., 2002).

αS is also associated with pathological lesions in other neurodegenerative diseases, sometimes involving nonneuronal cells, such as the glial cytoplasmic inclusions found in multiple system atrophy (MSA), a sporadic, progressive neurological disorder characterized by parkinsonism, cerebellar dysfunction, autonomic impairment, and pyramidal signs (Gai et al., 1998; Gilman et al., 1999; Spillantini et al.,

* Corresponding author at: Department of Neurology and Neurobiology of Aging, Kanazawa University Graduate School of Medical Science, 13-1 Takara-Machi, Kanazawa 920-8640, Japan. Tel.: +81 76 265 2290; fax: +81 76 234 4253.
E-mail address: m-yamada@med.kanazawa-u.ac.jp (M. Yamada).

0197-4580/$ – see front matter © 2012 Elsevier Inc. All rights reserved.
10.1016/j.neurobiolaging.2011.10.015

1998). A recent study in mice demonstrated that overexpression of αS in oligodendrocytes resulted in MSA-like degeneration in the central nervous system (CNS) (Yazawa et al., 2005). Convergent biochemical and genetic evidence suggests that the assembly of αS is an important and, probably, seminal step in the development of Lewy body diseases (LBD) including PD, DLB, and other α-synucleinopathies such as MSA.

Based on the nucleation-dependent polymerization model to explain the mechanism of αS assembly (Wood et al., 1999) in vitro, we and other groups previously reported that some antioxidants such as wine-related polyphenols, curcumin and rifampicin, inhibit formation of αS fibrils (fαS), as well as destabilize preformed fαS in vitro (Li et al., 2004; Ono and Yamada, 2006; Zhu et al., 2004).

The conversion of αS occurs via a multiple-step process involving nonfibrillar aggregates such as protofibrils or oligomers on αS assembly pathway (Caughey and Lansbury, 2003). As in the case of amyloid β-protein (Aβ), there is mounting evidence that protofibrils or oligomers of αS are more toxic than fαS on the pathway to fibril formation (Lashuel et al., 2002; Outeiro et al., 2008; Volles and Lansbury, 2003). If so, the most efficacious therapeutic agents would target the assembly or neurotoxic activity of these structures.

Melatonin (Mel), a secretory product of the pineal gland, is involved in the regulation of circadian and seasonal rhythms, in oncostasis, and in inducing osteoblast differentiation (Pévet et al., 2006; Reiter, 1991) (Fig. 1). Furthermore, Mel is superior to vitamin C and E in protecting from oxidative damage and in scavenging free radicals (López-Burillo et al., 2003). Recently, Ishido reported that Mel protected the neural cells from neurotoxicants by inhibition of both caspase-3/7 activation and disruption of the mitochondrial transmembrane potential (Ishido, 2007). He also reported that Mel inhibits αS assembly by using immunostaining (Ishido, 2007).

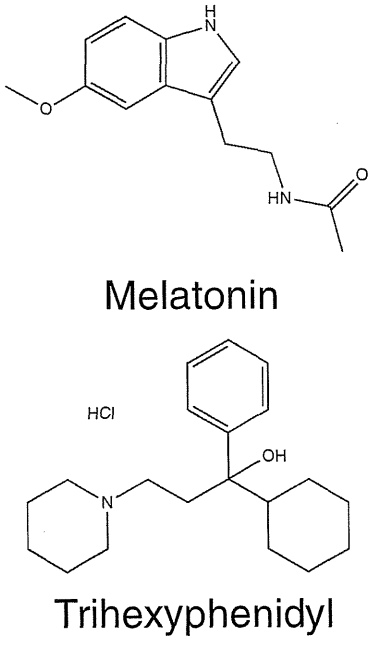

Fig. 1. Structures of melatonin and trihexyphenidyl.

In the studies reported here, we sought to determine whether Mel affected αS conformational dynamics and assembly, and whether these effects correlated with αS cytotoxicity. We treated αS with Mel and then monitored assembly and toxicity using a combination of circular dichroism spectroscopy (CD), photoinduced crosslinking of unmodified proteins (PICUP), size-exclusion chromatography (SEC), thioflavin S (ThS) binding, electron microscopy (EM), atomic force microscopy (AFM), and 3-[4,5-dimethylthiazol-2-yl]-2,5-diphenyltetrazolium bromide (MTT) metabolism. The results show potent inhibitory effects at all stages of peptide assembly.

2. Methods

2.1. Chemicals and reagents

Chemicals were obtained from Sigma-Aldrich, Co. (St. Louis, MO, USA) and were of the highest purity available. Water was produced using a Milli-Q system (Millipore Corp., Bedford, MA, USA).

2.2. Preparation of αS and fαS solutions

The αS and fαS solutions were prepared as described previously (Ono and Yamada, 2006). Briefly, αS (lot numbers 121303AS and 50306AS) was purchased from Recombinant Peptide Technologies, LLC (Bogart, GA, USA). To prepare αS for study, αS peptide was dissolved at 70 μM in 20 mM Tris buffer, pH 7.4. After sonication for 1 minute in a bath sonicator, the αS solution was centrifuged for 10 minutes at 16,000*g*. Fresh, nonaggregated fαS was obtained by polymerizing fresh αS just before the destabilization reaction. In the following experiment, the concentration of fαS in the final reaction mixture was regarded as 70 μM. A stock solution of glutathione S-transferase (GST; Sigma-Aldrich) was prepared by dissolving the lyophilizate to a concentration of 250 μM in 60 mM NaOH. Prior to use, aliquots were diluted 10-fold into 20 mM Tris buffer, pH 7.4.

2.3. Peptide aggregation

αS solutions were prepared as specified above and then 0.5-mL aliquots were placed in 1-mL microcentrifuge tubes. We selected trihexyphenidyl hydrochloride (Tri) (Fig. 1) which does not have inhibitory activity on αS aggregation as negative control (Ono et al., 2007). Mel and Tri were dissolved in ethanol to a final concentration of 2.5 mM and then diluted with 20 mM Tris, pH 7.4, 100 mM NaCl to produce concentrations of 50 and 500 μM. One-half mL of each compound then was added to separate tubes of αS, yielding final αS concentrations of 70 μM and final inhib-

itor concentrations of 25 and 250 μM. Compound:peptide ratios thus were 5:14 at the lower compound concentration and 25:7 at the higher compound concentration. Control tubes with peptide alone received 0.5 mL of buffer. The tubes were incubated at 37 °C for 0–6 days with agitation. We note that for each sample at each point analyzed, aliquots used for different experiments (see below) generally all came from the same tube of αS, ensuring that valid correlations could be made among the data obtained.

2.4. Fibrils destabilizing assay

fαS solutions were prepared as specified above and then 0.5-mL aliquots were placed in 1-mL microcentrifuge tubes. Compound preparation was similar to that of "Peptide aggregation." One-half mL of each compound then was added to separate tubes of αS, yielding final fαS concentrations of 70 μM and final inhibitor concentrations of 25 and 250 μM. Compound:peptide ratios thus were 5:14 at the lower compound concentration and 25:7 at the higher compound concentration. Control tubes with peptide alone received 0.5 mL of buffer. The tubes were incubated at 37 °C for 0–6 hours without agitation.

2.5. ThS fluorescence

The reaction mixture contained 5 mM ThS (MP Biomedicals, LLC, Irvine, CA, USA) and 50 mM of glycine-NaOH buffer, pH 8.5. After vortexing briefly, fluorescence was determined 3 times at intervals of 10 seconds using a Hitachi F-2500 fluorometer (Tokyo, Japan). Excitation and emission wavelengths were 440 and 521 nm, respectively. Sample fluorescence was determined by averaging the 3 readings and subtracting the fluorescence of a ThS blank.

2.6. CD

CD spectra of αS:compound mixtures were acquired immediately after sample preparation or after 1–6 days of incubation. CD measurements were made by removing a 200-μL aliquot from the reaction mixture, adding the aliquot to a 1-mm path length CD cuvette (World Precision Instruments, Sarasota, FL, USA), and acquiring spectra in a J-805 spectropolarimeter (Jasco, Tokyo, Japan). The CD cuvettes were maintained on ice prior to introduction into the spectrometer. After temperature equilibration, spectra were recorded at 22 °C from 190 to 260 nm at 0.2-nm resolution with a scan rate of 100 nm/minute. Ten scans were acquired and averaged for each sample. Raw data were manipulated by smoothing and subtraction of buffer spectra according to the manufacturer's instructions.

2.7. Protofibril formation

Prefibrillar intermediates, termed "protofibrils" (Conway et al., 1998, 2000; Wood et al., 1999) were defined as the material eluting in the void volume of the column by SEC as proposed previously (Volles et al., 2001). To study protofibril formation and the effects of compounds on it, we incubated αS according to the aggregation protocol above. Periodically during the 6-day incubation period, solutions were centrifuged at 16,000*g* for 5 minutes and then 200 μL of the supernatant was fractionated by SEC at a flow rate of 0.5 mL/minute on a Superdex 75 column (GE Healthcare BioSciences AB, Uppsala, Sweden) attached to a Waters 515 HPLC pump and a Waters 2489 UV/Visible detector (Waters, Milford, MA, USA). The void volume peak of protofibrils was detected and recovered at an elution time of 14 minutes by ultraviolet absorbance at 254 nm.

2.8. EM

A 10-μL aliquot of each sample was spotted onto a glow-discharged, carbon-coated formvar grid (Okenshoji, Co, Ltd, Tokyo, Japan) and incubated for 20 minutes. The droplet then was displaced with an equal volume of 2.5% (vol/vol) glutaraldehyde in water and incubated for an additional 5 minutes. Finally, the peptide was stained with 8 μL of 1% (vol/vol) filtered (0.2 μm) uranyl acetate in water (Wako Pure Chemical Industries, Ltd, Osaka, Japan). This solution was wicked off and then the grid was air-dried. Samples were examined using a JEM-1210 transmission electron microscope (JEOL Ltd., Tokyo, Japan).

2.9. AFM

Peptide solutions were characterized using a Nanoscope IIIa controller (Veeco Digital Instruments, Santa Barbara, CA, USA) with a multimode scanning probe microscope equipped with a JV (J-type vertical) scanner. All measurements were carried out in the tapping mode under ambient conditions using single-beam silicon cantilever probes. A 10-μL aliquot of each sample was spotted onto freshly cleaved mica (Ted Pella, Inc., Redding, CA, USA), incubated at room temperature for 5 minutes, rinsed with water, and then blown dry with air. At least 4 regions of the mica surface were examined to confirm the homogeneity of the structures throughout the sample. Mean particle heights were analyzed by averaging the measured values of 8 individual cross-sectional line scans from each image only when the particle structure was confirmed.

2.10. Chemical crosslinking and determination of oligomer frequency distributions

Immediately after their preparation, samples were crosslinked using PICUP, as described (Bitan et al., 2001). Briefly, to 18 μL of protein solution was added 1 μL of 1 mM tris(2,2′-bipyridyl)dichlororuthenium (II) (Ru(bpy)) and 1 μl of 20-mM ammonium persulfate (APS). The final protein:tris(2,2′-bipyridyl)dichlororuthenium (II):ammonium persulfate molar ratios of αS were 0.32:1:20. The mixture was irradiated for 1 second with visible light and then the reaction was quenched with 10 μL of tricine sample buffer (Invitrogen, Carlsbad, CA, USA) containing 5% (vol/vol) β-mercaptoethanol. Determination of the frequency distribution of monomers and oligomers was accomplished using

sodium dodecyl sulfate polyacrylamide gel electrophoresis (SDS-PAGE) and silver staining, as described (Bitan et al., 2001). Briefly, 20 μL of each crosslinked sample was electrophoresed on a 10%–20% gradient tricine gel and visualized by silver staining (SilverXpress, Invitrogen). Non-crosslinked samples were used as controls in each experiment. Densitometry was performed with a luminescent image analyzer (LAS 4000 mini, Fujifilm, Tokyo, Japan) and image analysis software (Multigauge v. 3.2, Fujifilm). The intensity of each band in a lane from the SDS gel was normalized to the sum of the intensities of all the bands in that lane, according to the formula

$$R_i = I_i / \sum_{i=1}^{n} I_i \times 100\,(\%)$$

where R_i is the normalized intensity of band i and I_i is the intensity of each band i. R_i varies from 0 to 100. To calculate the oligomer ratio, the sum of oligomer intensities of αS with 1, 2.5, 5, 10, 25, and 250 μM Mel was divided by the sum of oligomer intensities without each compound. The effective concentration (EC50) was defined as the concentration of Mel to inhibit αS oligomerization to 50% of the control value. EC50 was calculated by sigmoidal curve fitting, using GraphPad Prism software (version 4.0a, GraphPad Software, Inc., San Diego, CA, USA).

2.11. Primary neuronal culture

Primary cultures of mesencephalon and neostriatum were obtained from embryos (E 13–14) of C57BL/6J mouse. Cultures were performed as described previously (Goto et al., 1997; Mochizuki et al., 1994), with the following modifications: the mesencephalon and neostriatum were dissected out and dissociated, then seeded at a density of 2.1×10^5 cells per well (mesencephalon: 0.25×10^5, neostriatum: 1.85×10^5) (90-μL total volume per well) on 96-well plates (Nalge Nunc International K.K., Tokyo, Japan) with 5% polyethylenimine (Sigma Chemical Co., St. Louis, MO, USA). The cultures were kept in a 37 °C incubator in a humidified atmosphere containing 95% O_2/5% CO_2. After incubation in F12/DMEM (Gibco, Grand Island, NY, USA) 10% fetal bovine serum for 48 hours, the medium was changed to F12/DMEM (Gibco) 5% (vol/vol) calf serum, 5% (vol/vol) horse serum to prepare cells for assay. For neuron-rich cultures, on Day 5, cytosine arabinoside (Sigma Chemical Co.) (10 μM) was added for 48 hours to limit the growth of glial cells. F12/DMEM (Gibco) 5% (vol/vol) calf serum, 5% (vol/vol) horse serum was changed at Day 7 in vitro, at which point toxicity assays were done.

2.12. MTT assay

Mel and αS with either 0 μM or 25 μM Mel were incubated in 20 mM Tris, pH 7.4, 100 mM NaCl at 37 °C for 0, 2, or 6 days with agitation prior to the addition of a 10-μL aliquot of the sample to the primary neurons of mesencephalon and neostriatum. Cells were treated for 48 hours with a final concentration of 2.5 μM Mel alone, 7 μM αS alone, or with αS plus 2.5 μM Mel. Peptide:compound ratios of αS were 2.8. To determine toxicity, we used Cell Counting Kit-8 (CCK-8; Dojindo Molecular Technologies, Inc., Rockville, MD, USA). In practice, the "zero time" samples were equivalent, as all components were mixed with cells at the same time.

To determine toxicity, we added 10 μL of CCK-8 solution (Dojindo Molecular Technologies, Inc.) to each well of the microtiter plate and the plate was incubated in the CO_2 incubator for an additional 4 hours. After incubation, CCK-8 reduction was assessed by measuring absorption at 450 nm (corrected for background absorbance at 650 nm) using a Bio-Rad microplate reader (Bio-Rad, Vermont). Control included media with 20 mM Tris, pH 7.4, 100 mM NaCl ("negative"). Five replicates were done for each treatment group and reported as mean ± standard error. Cell viability = $(A_{sample})/(A_{medium}) \times 100$, where A_{sample} and A_{medium} were absorbance values from Mel alone or αS-containing samples, and medium, respectively.

2.13. Statistical analysis

One-way factorial analysis of variance (ANOVA) followed by Bonferroni post hoc comparisons were used to determine statistical significance among data sets. These tests were implemented within GraphPad Prism software (version 4.0a, GraphPad Software, Inc.). Significance was defined as $p < 0.05$.

3. Results

3.1. Mature fibril formation

To determine whether fibril formation was affected by Mel, we used ThS to monitor temporal changes in the β-sheet content in samples of αS in the absence or presence of Mel. ThS fluorescence is not a measure of fibril content per se, but because β-sheet formation correlates with fibril formation, ThS fluorescence is a useful surrogate marker (LeVine, 1993, 1999; Naiki and Nakakuki, 1996). The ThS studies also allowed us to determine the kinetics of peptide assembly, providing information on nucleation and elongation phases of αS assembly. We included Tri (Fig. 1) here as a negative control because, like Mel, it is an aromatic compound and we previously confirmed that Tri did not affect αS assembly (Ono et al., 2007).

In the absence of compounds, αS displayed a quasi-sigmoidal binding curve characterized by a lag time of 1 day, a period of successively increasing ThS binding for 3 days, and a binding plateau occurring after 4 days (Fig. 2A and B)—results consistent with the well-known nucleation-dependent polymerization model of αS assembly (Wood et al., 1999). When αS was incubated with Tri, either at a compound:peptide ratio of 5:14 or 25:7, the binding curves were identical to that of the untreated peptide, within experimental error (Fig. 2A). In contrast, significant effects were produced by Mel (Fig. 2B), such as a concentration-dependent increase in lag time, decrease in β-sheet growth rates, and decrease in final β-sheet levels (Table 1).

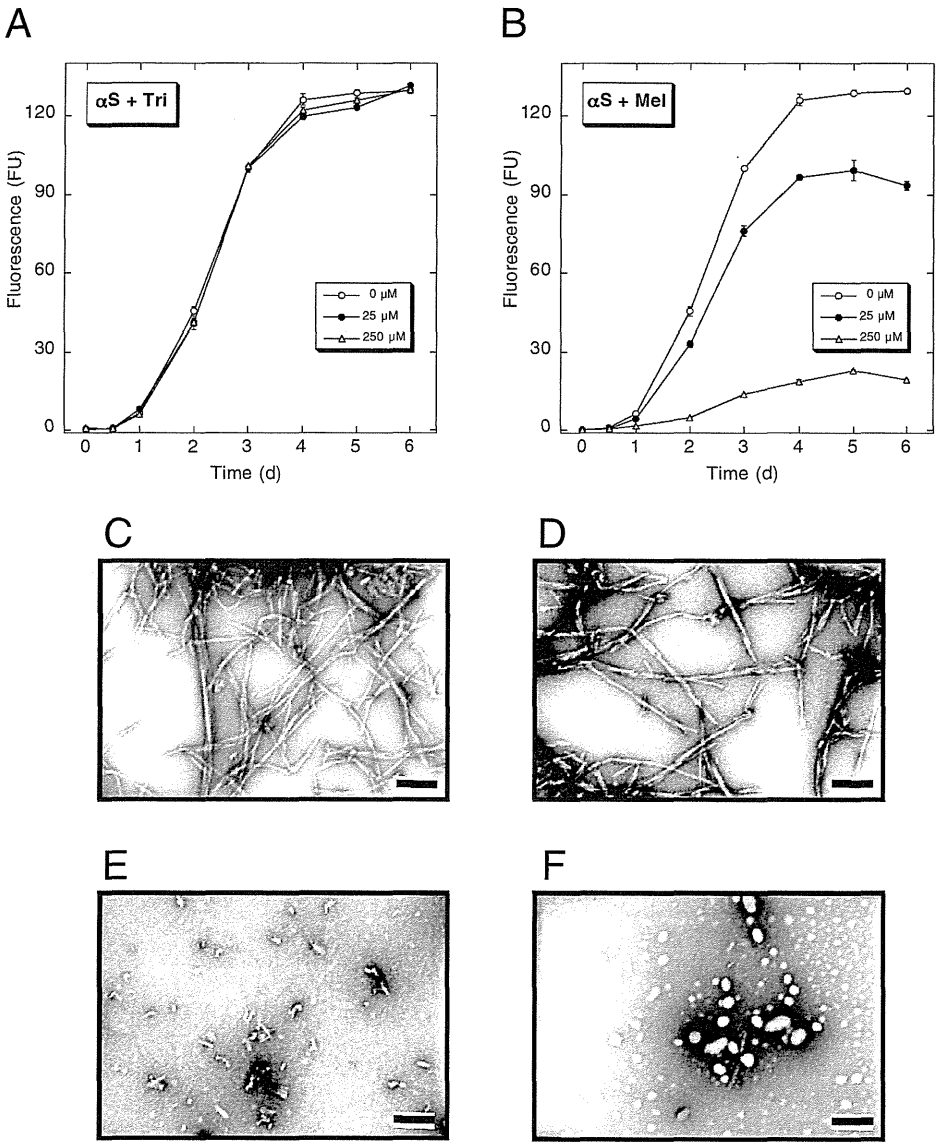

Fig. 2. Melatonin inhibits α-synuclein (αS) fibril formation. (A, B) thioflavin S (ThS) binding; 70 μM αS was incubated for 6 days at 37 °C in 20 mM Tris buffer, pH 7.4, in the presence of 0 (○), 25 (●), or 250 (Δ) μM trihexyphenidyl hydrochloride (Tri) (A) or melatonin (Mel) (B). Periodically, aliquots were removed and ThS binding levels were determined. Binding is expressed as mean fluorescence (in arbitrary fluorescence units [FU]) ± standard error. Each figure comprises data obtained in 3 independent experiments. (C–F) αS assembly morphology. Electron microscopy (EM) was used to determine the morphologies of assemblies of αS incubated at 37 °C for 6 days in 20 mM Tris buffer, pH 7.4. αS peptide was incubated in buffer alone (C) or in the presence of 250 μM Tri (D), 25 μM Mel (E), or 250 μM Mel (F). Scale bars indicate 100 nm.

Using EM, we determined the morphology of the αS assemblies when maximal ThS binding was observed. Classical amyloid-like fibrils were observed in samples of untreated αS (Fig. 2C). The fαS were nonbranched, helical filaments with diameters of 10 nm as reported before (Conway et al., 2000; Ono and Yamada, 2006). The addition of Tri (here for the higher, 250 μM concentration) did not alter the assembly of αS (Fig. 2D). In contrast to the results with Tri, strong inhibition of fibril formation was observed in Mel-treated samples. At substoichiometric concentration (compound:peptide ratio of 5:14), treatment of αS with 25 μM Mel clearly reduced fibril number and many short, shared fibrils were observed (Fig. 2E). Treatment of αS with 250 μM Mel markedly reduced fibril number and increased the relative numbers of short fibrils and amorphous aggregates (Fig. 2F).

3.2. Destabilization of preformed fibrils

We used ThS to monitor temporal changes in β-sheet content in samples of preformed fαS in the absence or presence of Mel.

Table 1
Kinetics of α-synuclein (αS) assembly

Sample	Lag time (d)[a]	Growth rate (FU/d)[b]	Maximum intensity (FU)[c]
αS	1.2	54.6	129.3
αS + 25 μM Tri	1.2	58.8	131.2
αS + 250 μM Tri	1.3	59.4	129.8
αS + 2.5 mM Tri	1.2	53.4	127.6
αS + 25 μM Mel	1.2	43.2	99.3
αS + 250 μM Mel	1.4	8.8	22.8
αS + 2.5 mM Mel	1.9	5.4	10.5

Key: d, day; FU, fluorescence units; Mel, melatonin; Tri, trihexyphenidyl hydrochloride.

[a] Lag time was defined as the point of intersection with the abscissa of the line determined by the pseudolinear portion of the fluorescence progress curve, according to Evans et al., 1995.

[b] Growth rate was determined by line fitting to the pseudolinear segment of the ascending portion of the fluorescence progress curve.

[c] Determined by visual inspection.

In the absence of compounds, ThS fluorescence of fαS was almost unchanged during 6 hours (Fig. 3A and B) as previously described (Ono and Yamada, 2006). After incubation of fαS with Tri, either at a compound:peptide ratio of 5:14 or 25:7, the ThS fluorescence was similar to that of the untreated peptide, within experimental error (Fig. 3A). In contrast, Mel showed significant destabilization effects (Fig. 3B). These strong effects of Mel were in a concentration-dependent manner, suggesting decrease of final β-sheet levels.

Using EM, we determined the morphological change of the preformed fαS with time course. Classical amyloid-like fibrils were observed in samples of fresh fαS (Fig. 3C). At substoichiometric concentration (compound:peptide ratio of 5:14), treatment of fαS with 25 μM Mel for 6 hours clearly reduced fibril number and many short, shared fibrils were observed (Fig. 3D). After incubation of fresh fαS with 250 μM Mel (compound:peptide ratio of 25:7) for 1 hour, many sheared fibrils were observed (Fig. 3E). At 6 hours, the number of fibrils was reduced markedly, and small amorphous aggregates were occasionally observed (Fig. 3F). In contrast to the results with Mel, Tri did not have a destabilizing effect at 250-μM concentration (Fig. 3G).

3.3. Protofibril formation

To determine the effect of Mel, we monitored the process of protofibril formation by SEC. Incubation of αS alone produced chromatograms containing 2 predominant peaks, the first eluting at 14 minutes and the second eluting at 18 minutes (Fig. 4A). We confirmed that the second peak shows a monomer band of αS, and called this nominal monomer fraction low molecular weight (LMW) αS. On the other hand, the first peak (void fraction) did not include the small bands because SDS-stable larger aggregates composed mainly of protofibrils could not be moved into the separating gel (Fig. 4B).

To quantitatively compare the temporal changes in protofibril and LMW contents among samples, we integrated the areas under the first and second peaks, and graphed them versus time (Fig. 4C and D). Untreated αS displayed a monotonic increase in protofibril amount until plateau levels were reached at 4 days (Fig. 4C). When αS was incubated with Tri at a compound:peptide ratio of 25:7, protofibril formation occurred with a kinetics indistinguishable from that of αS alone. In contrast, highly significant inhibition of protofibril formation was observed in the presence of Mel. Small increases in protofibril amount were observed until 3 days, at which point the amount reached plateau at a level fourfold lower than that of αS alone. On the other hand, untreated αS displayed a monotonic decrease in LMW amount until minimal levels were reached at 4 days (Fig. 4D). When αS was incubated with Tri at a compound:peptide ratio of 25:7, the LMW amount changed with a kinetics indistinguishable from that of αS alone. In contrast, highly significant inhibition of the decrease of LMW amount was observed in the presence of Mel. Small decreases in LMW amount were observed until 4 days, at which point the amount plateaued at a level fourfold higher than that of αS alone.

To determine the morphology of the assemblies present after αS incubation with or without compounds, we examined samples of void fraction after 6 days of incubation using EM. Untreated αS (Fig. 4E) produced short, relatively narrow (7–8 nm) structures displaying periodic substructure reminiscent of beaded strings. Similar structures were observed in samples that had been treated with Tri (Fig. 4F). However, grids of αS samples treated with Mel contained few structures and these structures were composed of fewer subunits than were structures formed in the presence of Tri or in the absence of added compounds (compare Fig. 4G with Fig. 4E and F).

3.4. αS oligomerization

We next determined whether Mel blocked protofibril formation by low-order αS oligomers or whether oligomerization itself was blocked. We applied PICUP, a photochemical crosslinking method that is rapid, efficient, requires no structural modification of peptide (for a review, see Bitan and Teplow, 2004), and accurately reveals the oligomerization state of Aβ as well as αS (Bitan and Teplow, 2004; Li et al., 2006). In the absence of crosslinking, there was only αS monomer (Fig. 5A, lane 2). After crosslinking, αS existed as a mixture of monomers and oligomers of order 2–4 (Fig. 5A, lane 3).

The oligomerization of αS in the presence of Tri produced oligomer distribution indistinguishable from that of αS alone (Fig. 5A, lane 4). A 10-fold increase in the compound:peptide ratio did not alter the distribution significantly (Fig. 5A, lane 5).

Mel mixed with αS at 25 μM (compound:peptide ratio of 5:14) blocked oligomerization almost completely (Fig. 5A,

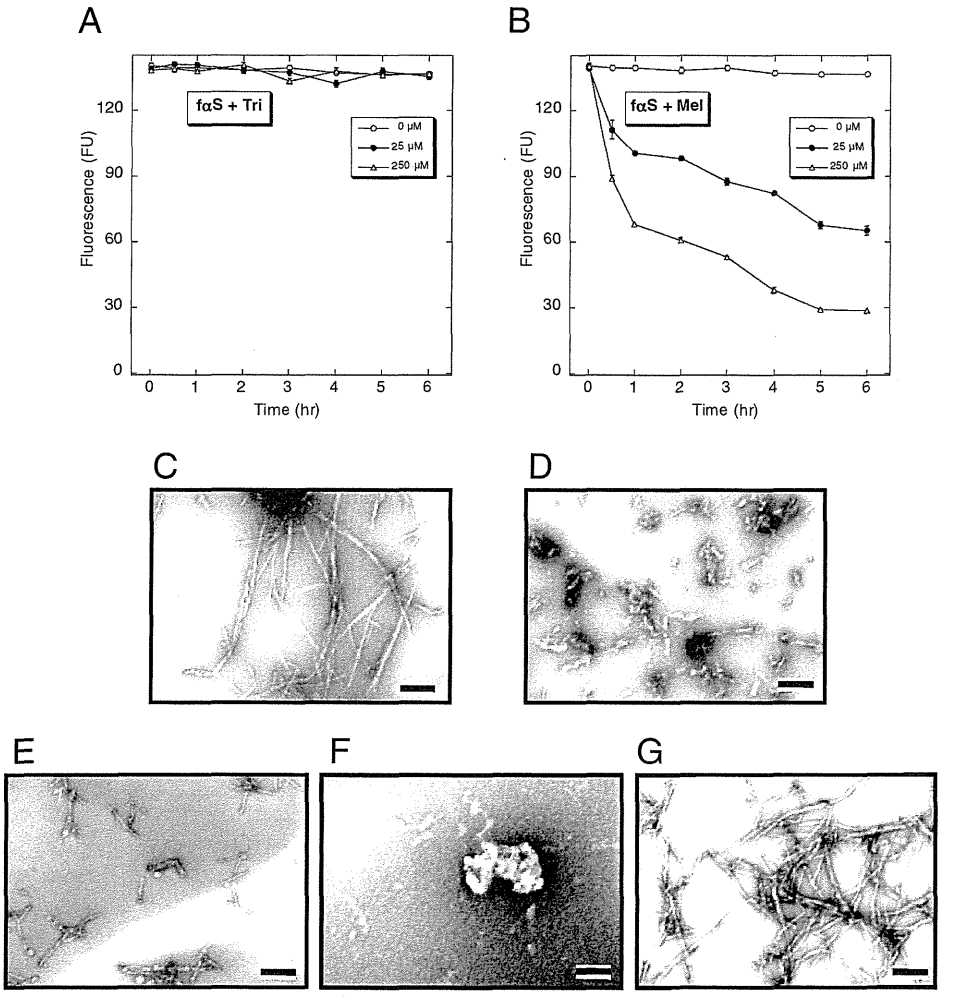

Fig. 3. Melatonin destabilizes preformed α-synuclein (αS) fibrils. (A, B) Thioflavin S (ThS) binding; 70 μM αS fibrils was incubated for 6 hours at 37 °C in 20 mM Tris buffer, pH 7.4, in the presence of 0 (○), 25 (●), or 250 (Δ) μM trihexyphenidyl hydrochloride (Tri) (A) or melatonin (Mel) (B). Periodically, aliquots were removed and ThS binding levels were determined. Binding is expressed as mean fluorescence (in arbitrary fluorescence units [FU]) ± standard error. Each figure comprises data obtained in 3 independent experiments. (C–G) αS destabilization morphology. Electron microscopy (EM) was used to determine the morphologies of destabilization of αS fibrils incubated at 37 °C for 6 hours in 20 mM Tris buffer, pH 7.4. αS fibrils was incubated in the presence of 25 μM Mel (D), 250 μM Mel (C, E, F), or 250 μM Tri (G) for 0 (C), 1 (E), or 6 hours (D, F, G). Scale bars indicate 100 nm.

lane 6). Increasing the compound:peptide ratio 10-fold produced similar levels of inhibition (Fig. 5A, lane 7). We also confirmed dose-dependency of this inhibition (Supplementary Fig. 1A and B). Mel exhibited an inhibitory effect on αS oligomerization at 2.5 μM (compound:peptide ratios of 1:28), and almost completely inhibited it at 10 μM (compound: peptide ratios of 2:14) (Supplementary Fig. 1A and B). EC50 of Mel for the oligomerization of αS was 2.7 μM.

The strong inhibition of αS oligomerization could have resulted from an effect of the inhibitor on the PICUP chemistry itself. To evaluate this possibility, crosslinking reactions also were performed on GST (26 kDa), a positive control for the crosslinking chemistry (Fancy and Kodadek, 1999). Uncrosslinked GST exhibited an intense monomer band and a relatively faint dimer band (Fig. 5B, lane 2). Crosslinking produced an intense dimer band, expected because GST exists normally as a homodimer, as well as higher order crosslinked species (Fig. 5B, lane 3). No alterations in GST crosslinking were observed in the presence of Tri at either of the 2 compound:protein ratios tested, 1:1 (Fig. 5B, lane 4) or 10:1 (Fig. 5B, lane 5). Similar distributions were observed with Mel at both 1:1 and 10:1 ratios (Fig. 5B, lanes 6 and 7). A chemistry effect cannot explain the strong inhibition of αS oligomerization, and the lack of inhibition of GST oligomerization.

To determine the morphology of the small assemblies present following PICUP of αS with or without compounds, we examined αS samples using AFM. The height of untreated αS was 0.56 ± 0.36 nm (n = 47) (Fig. 5C). After PICUP, the height of αS oligomers became 1.53 ± 0.77 nm

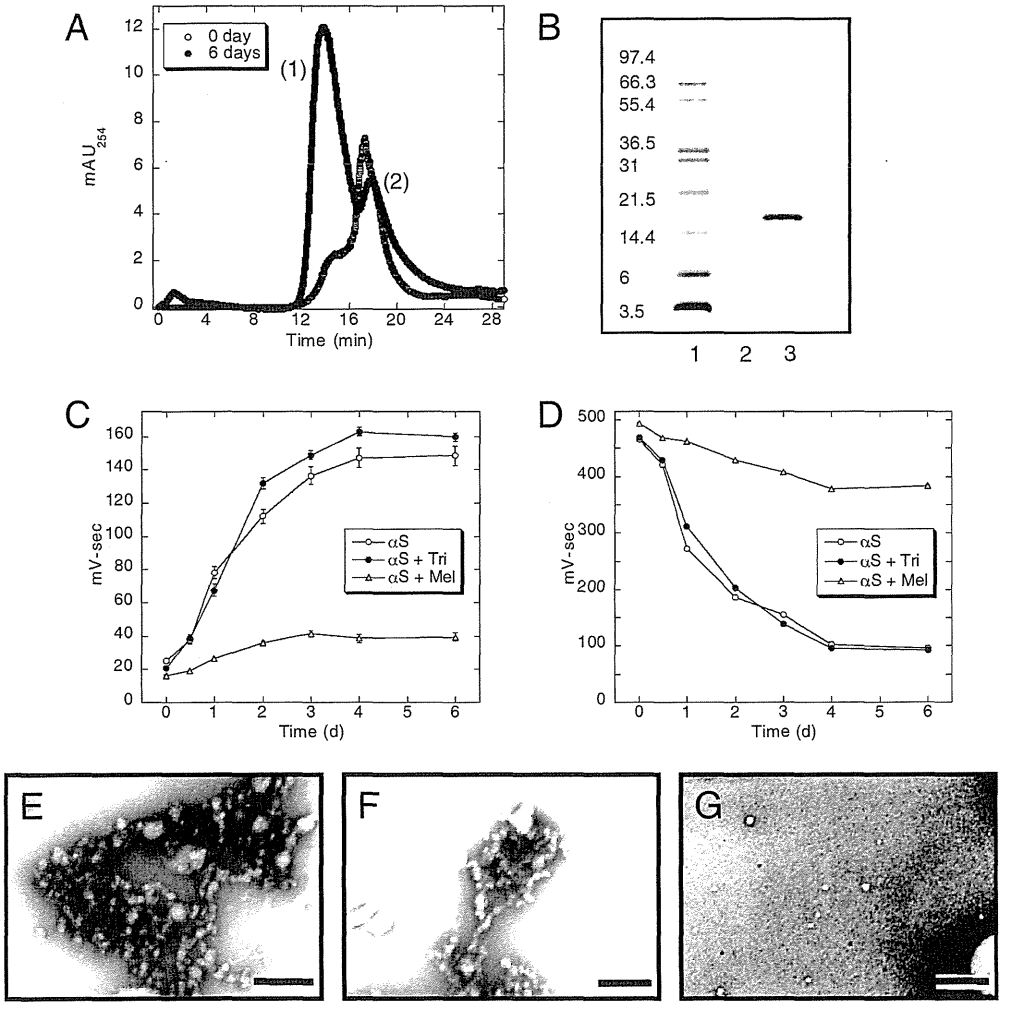

Fig. 4. Protofibril formation. α-Synuclein (αS) peptides were incubated alone (○) or in the presence of 250 μM trihexyphenidyl hydrochloride (Tri) (●) or melatonin (Mel) (Δ). Periodically during incubation, aliquots were analyzed by size-exclusion chromatography (SEC) to quantify protofibril formation. (A) SEC of αS incubated alone at 37 °C during 0–6 days reveals a protofibril peak eluting at 14 minutes, along with an low molecular weight (LMW) αS peak at 18 minutes. These 2 peaks are followed by sodium dodecyl sulfate polyacrylamide gel electrophoresis (SDS-PAGE) and silver staining (B). Lane 1, molecular weight markers; 2, peak; (1) 3, peak (2). The areas under the protofibril (C) and LMW (D) peaks (see A) were integrated to determine temporal changes in protofibril and LMW amounts in samples. Areas are expressed as mean area ± standard error. Each figure comprises data obtained in 3 independent experiments. (E–G) Protofibrils morphology. Electron microscopy (EM) was used to determine the morphologies of protofibrils obtained by SEC after incubation of αS (E–G) at 37 °C for 6 days in 20 mM Tris buffer, pH 7.4. αS peptides were incubated in buffer alone (E) or in the presence of 250 μM Tri (F) or Mel (G). Scale bars indicate 100 nm.

(n = 29) (Fig. 5D). When αS was crosslinked with Tri at a compound:peptide ratio of 25:7, the height of treated αS was 1.42 ± 0.53 nm (n = 29) (Fig. 5E). When αS was crosslinked with Mel at a compound:peptide ratio of 5:14, the height of treated αS was 0.57 ± 0.44 nm (n = 37) (Fig. 5F).

3.5. αS secondary structure dynamics

The oligomerization studies revealed effects of Mel at the initial stages of peptide self-association. To probe the secondary structure of αS at this stage, and to determine if Mel affected later conformational properties of the peptide monomer or its oligomers, CD was used to monitor peptide assembly (Fig. 6). αS, incubated alone, produced initial spectra characteristic of statistical coils (Fig. 6A). The major feature of these spectra was a large magnitude minimum centered at 198 nm. A significant conformational transition occurred during the subsequent 3 days, producing the spectra which was a substantial minimum centered at 216 nm, indicative of β-sheet structure. Similar conformational transition was observed in populations of αS in the presence of Tri (Fig. 6B). When Mel was mixed with αS at a compound:peptide ratio of 5:14, the secondary structure transition from statistical coil to mixture with predominant α-helix was observed (Fig. 6C). A 10-fold increase in the compound:peptide ratio produced almost complete

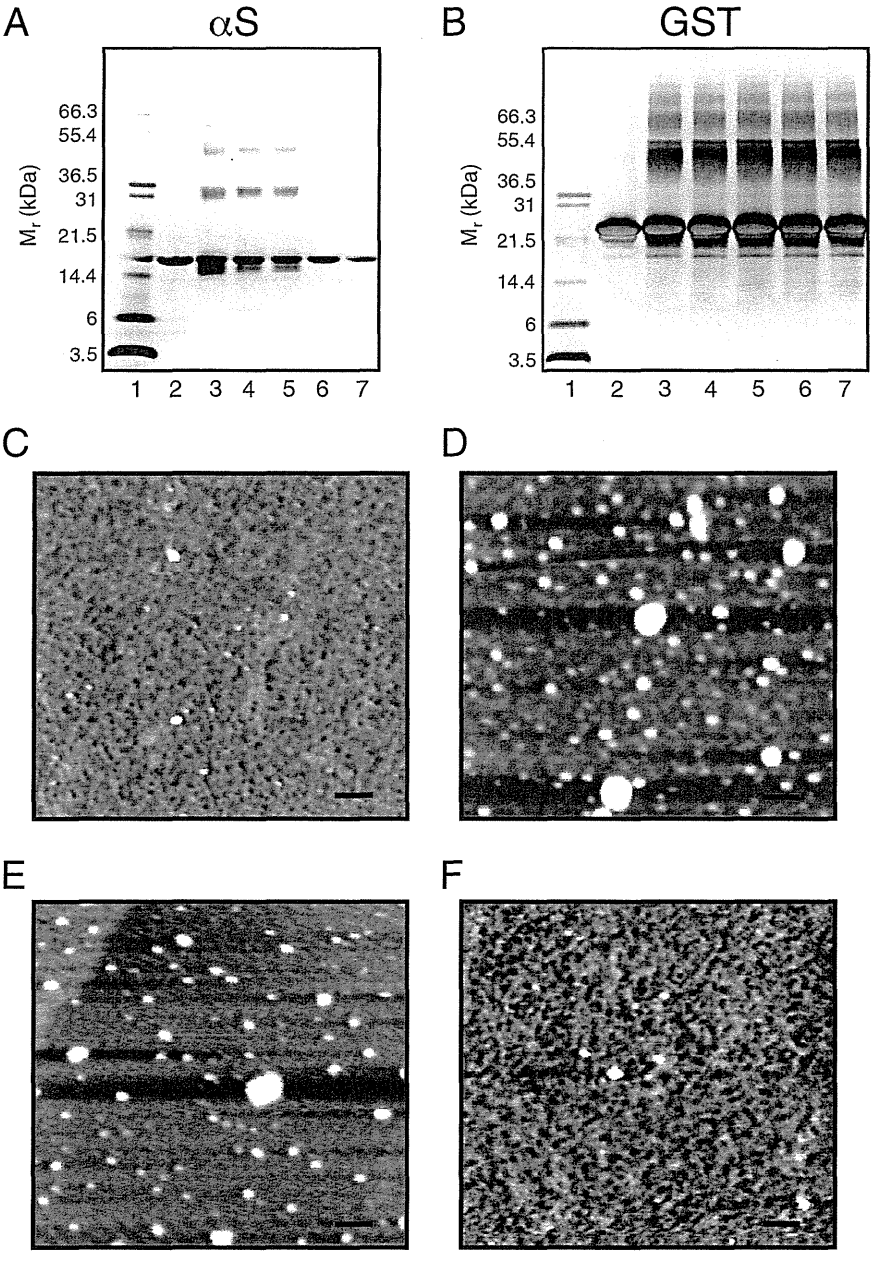

Fig. 5. α-Synuclein (αS) oligomerization. Photoinduced crosslinking of unmodified proteins (PICUP), followed by SDS-PAGE and silver staining, was used to determine the effects of melatonin (Mel) or trihexyphenidyl hydrochloride (Tri) on oligomerization of αS (A), or glutathione S-transferase (GST) (B). Lane 1, molecular weight markers; 2, proteins alone (no crosslinking); 3, proteins alone; 4, proteins plus Tri (25 μM); 5, proteins plus Tri (250 μM); 6, proteins plus Mel (25 μM); 7, protein plus Mel (250 μM). The gel is representative of 3 independent experiments. (C–F) Oligomer morphology. Atomic force microscopy (AFM) was used to determine the morphologies of oligomers obtained by PICUP of αS alone (no crosslinking) (C), αS alone (after crosslinking) (D), αS with 250 μM Tri (after crosslinking) (E), αS with 25 μM Mel (after crosslinking) (F). Scale bars indicate 100 nm.

inhibition (Fig. 6D), suggesting that Mel-treated αS revealed populations of conformers that were largely a statistical coil.

3.6. αS-mediated cellular toxicity

To investigate the ability of Mel to block αS-mediated cellular toxicity, we used primary mixed neurons obtained from mesencephalon and neostriatum to perform MTT assay to probe cellular metabolism. The experimental design was the protocol: incubating Mel only, αS alone, or αS with Mel for various times prior to addition to cells (Fig. 7). When cells were exposed to the samples, the assays proceeded as described elsewhere (Abe and Saito, 1998; Storch et al., 2004).

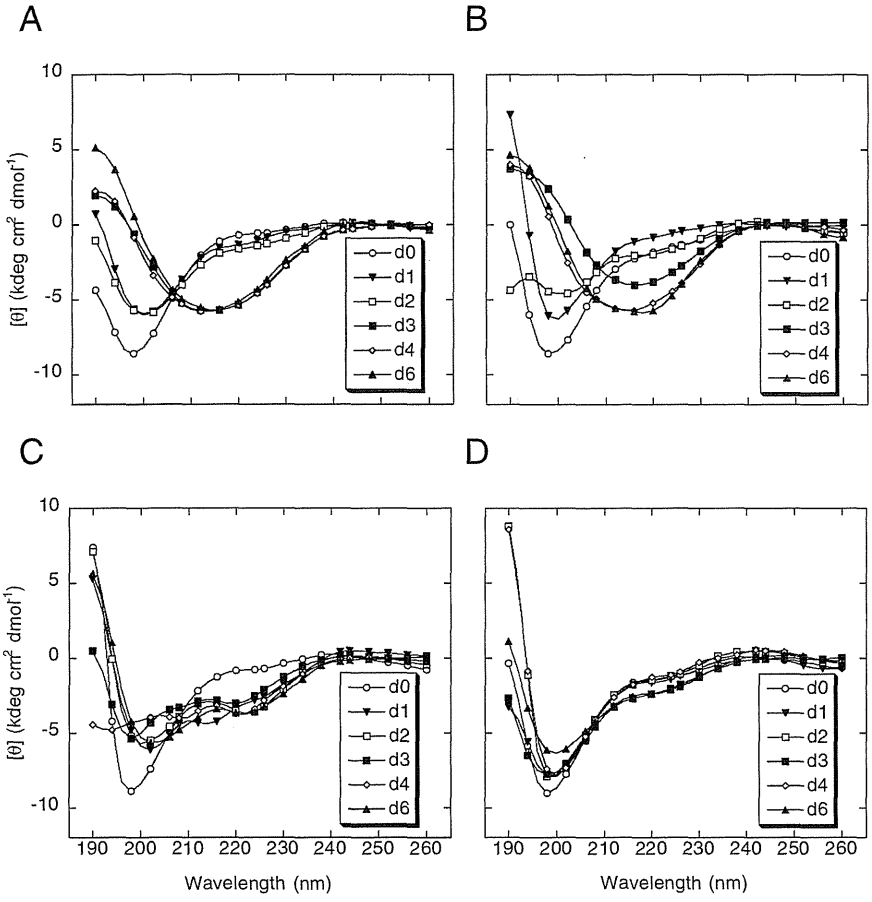

Fig. 6. α-Synuclein (αS) secondary structure dynamics. (A–D) 35 μM αS were incubated at 37 °C for 6 days in 20 mM Tris buffer, pH 7.4, in buffer alone (A) or in the presence of 250 μM trihexyphenidyl hydrochloride (Tri) (B), or 25 μM (C), or 250 μM melatonin (Mel) (D). Spectra were acquired immediately at the start of the incubation period, Day 0 (○), and after Days 1 (▼), 2 (□), 3 (□), 4 (◇), and 6 (▲). The spectra presented at each time are representative of those obtained during each of 3 independent experiments.

When αS alone was immediately added to the primary mixed neurons of mesencephalon and neostriatum, its cell viability was not significantly different from Mel only or buffer only (controls) (Fig. 7). The viability of cells with Mel-treated αS was also not significantly different from that of the controls. However, incubation of αS for 2 days, during which time oligomers, protofibrils, and fibril would be formed, produced aggregates that were significantly more toxic. Viability of cells with untreated αS was approximately 70%. Treatment of αS with Mel increased cell viability to approximately 86%, which was a highly significant increase relative to αS alone ($p < 0.01$) (Fig. 7). The same qualitative relationships among these experimental groups were observed after 6 days of incubation. Viability of cells with untreated αS was approximately 83%, which was significantly less toxic than that with αS after 2 days incubation ($p < 0.05$). Treatment of αS with Mel significantly increased cell viability to approximately 97% ($p < 0.01$) (Fig. 7).

4. Discussion

Mel is normally synthesized and secreted during the dark phase of the day. A primary function of Mel secretion is to convey information about daily cycles of light and darkness to body physiology (Srinivasan et al., 2005). A substantial body of evidence suggests that Mel may inhibit fibril formation by a variety of amyloidogenic proteins (Srinivasan et al., 2005). Aβ studies showed that Mel strongly inhibited the spontaneous formation of β-sheets and Aβ fibrils (Pappolla et al., 1998). The protective actions of Mel against Aβ neurotoxicity have been repeatedly confirmed (Poeggeler et al., 2001; Shen et al., 2002a, 2002b, 2002c). Furthermore, Mel inhibited the expected time-dependent elevation of Aβ in a transgenic mouse model of Alzheimer's amyloidosis (Matsubara et al., 2003).

Mel has been shown to attenuate arsenite-induced apoptosis via a reduction of aggregated αS levels in rat brain (Lin et al., 2007) by Western blot analysis. Similarly, Ishido reported that Mel inhibits maneb-induced assembly of αS in

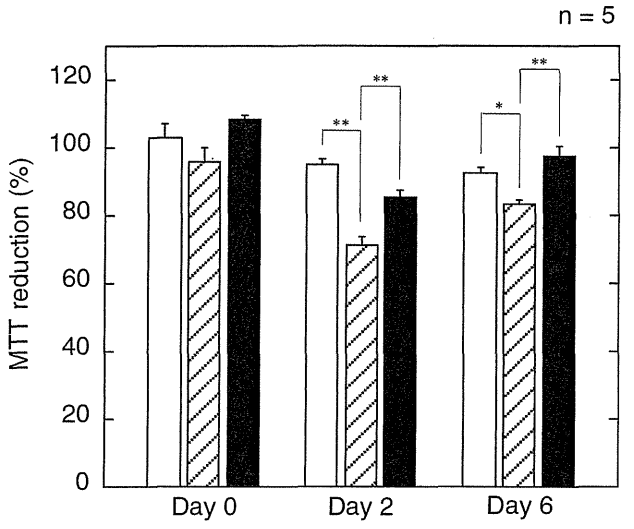

Fig. 7. 3-[4,5-dimethylthiazol-2-yl]-2,5-diphenyltetrazolium bromide (MTT) metabolism. α-Synuclein (αS) was incubated with or without melatonin (Mel) in 10 mM Tris, pH 7.4, at 37 °C for 0, 2, and 6 days prior to addition to primary mixed neurons comprised of mesencephalon and neostriatum. Effects of Mel only (open bars), untreated αS (cross-hatched bars), and Mel-treated αS (closed bars) on cell metabolism were determined fluorometrically using MTT 48 hours after sample addition. Each bar represents mean ± standard error. Statistical significance among groups was determined using 1-way fractional analysis of variance (ANOVA) and multiple comparison tests. Differences reaching statistical significance are noted by line segments between samples, along with their associated p values, where * signifies $p < 0.05$ and ** signifies $p < 0.01$.

rat pheochromocytoma cells investigated by immunostaining (Ishido, 2007). Thus, it is reasonable that Mel has an anti-misfolding effect for αS as well as for Aβ. We sought here to examine more deeply the mechanism of inhibition, a goal critical to accelerating knowledge-based strategies for inhibitor targeting and design.

We began by studying fibril formation in parallel with assessing assembly β-sheet content. EM and ThS experiments revealed that Mel strongly inhibited β-sheet and fibril formation by αS. Working backwards systematically along the αS assembly pathway, we found that Mel also was a highly effective inhibitor of protofibril formation and peptide oligomerization.

Some studies have sought to establish the relative importance of different types of αS assemblies in disease pathogenesis (for a recent review, see Caughey and Lansbury, 2003). For example, protofibrils have been linked to an A30P form of early-onset PD (Conway et al., 1998). Protofibrils forming annular structures may have pore-like properties and might damage membranes (Lashuel et al., 2002; Volles et al., 2001). A linear association/annealing of these spherical species, resembling an Aβ protofibril, was observed in the preparation of protofibrils (Conway et al., 2000). Morphology of void volume fraction gained by our SEC experiments was consistent with this report. The area of this fraction displayed monotonic increase until plateau with the incubation. Taken together, our data suggested that Mel strongly inhibits the protofibril formation. Thus, the ability of Mel to inhibit both fibril and protofibril formation suggests that it may be of value for therapeutic strategies targeting these 2 assembly types.

Most recently, new studies have revealed that low-order oligomeric forms of αS are also toxic and critical species (Outeiro et al., 2008; Paleologou et al., 2009; Tsigelny et al., 2008). Outeiro et al. have shown that formation of dimeric and oligomeric αS species, both of which are thought to precede the formation of larger intracellular inclusions, are central steps toward cytotoxicity which can be targeted through the activity of molecular chaperones, such as heat shock protein 70 (Hsp70) (Outeiro et al., 2008). Consistent with this result, toxicity is seen without heavily aggregated αS, and it has been suggested that soluble species mediate toxicity (Xu et al., 2002). It was reported that soluble spheroid oligomer has 1.5–3.0 nm in height by AFM studies (Apetri et al., 2006), being consistent with our results of AFM. Very recently, it was reported that αS exists physiologically as a helically folded tetramer that precedes αS misfolding and aggregation, suggesting that stabilization of the tetramer could reduce LBD pathogenicity (Bartels et al., 2011).

Recently, annular αS oligomers have been isolated from human brain samples of MSA (Pountney et al., 2004). A novel enzyme-linked immunosorbent assay (ELISA) method revealed an elevation of αS oligomer level in plasma samples obtained from PD patients compared with controls (El-Agnaf et al., 2006), and the levels of soluble oligomers of αS were higher in the DLB brain than in the brain of patients with Alzheimer's disease and the controls (Paleologou et al., 2009), which support the idea that oligomers are the toxic species. Interestingly, EC50 of Mel for the oligomerization of αS was 2.7 μM (compound:peptide ratios of 1 to approximately 26), suggesting that Mel especially has strong inhibitory effect on oligomerization of αS. The strong ability of Mel to block formation of low-order αS oligomers in our results suggests that it might also be of value for targeting what some have argued are the proximate neurotoxins in LBD (Outeiro et al., 2008; Paleologou et al., 2009; Tsigelny et al., 2008).

Our CD studies, in concert with ThS experiments, showed that Mel produced a conformer population comprising primarily statistical coils. Whether Mel stabilizes unfolded αS conformers or destabilizes folded conformers or oligomeric or fibrillar assemblies cannot be ascertained from the data extant. However, the consequences of Mel treatment in the αS system do appear to differ from those observed in certain other inhibitor:amyloidogenic protein systems. For example, Zhu et al. (2004) reported that the flavonoid baicalein stabilized a partially folded conformer of αS that existed within oligomeric assemblies. Conway et al. (2001) showed that dopamine or levodopa inhibits the fibrillization of αS filaments, presumably through stabiliza-

tion of αS into protofibrillar structures unable to form fibrils. Taniguchi et al. (2005) reported the formation of tau oligomers in the presence of phenothiazines, polyphenols, or porphyrins. In each of these cases, the inhibitors stabilized oligomeric states in which the respective protein maintained at least a partial fold. The ability of Mel to block αS monomer folding and, especially, oligomerization thus is a particularly important aspect of a mechanism underlying its effect.

The most important biological consequence of αS association is the production of neurotoxic assemblies. In the work reported here, assemblies of αS that were added to cultures of primary neurons caused significant cellular damage, as measured by effects on MTT metabolism. There are some reports that the increase of cell viability in MTT assay was consistent with the increase of tyrosine hydroxylase activity in the cells of mesencephalon (Nobre-Júnior et al., 2009) and neostriatum (Barrachina et al., 2003). Our results that nonaggregated αS is less toxic than aggregated αS as well as that intermediate aggregates are more toxic than final aggregates were not inconsistent with reports that early intermediates of αS are toxic and critical species (Outeiro et al., 2008; Paleologou et al., 2009; Tsigelny et al., 2008). Mel substantially reduced these toxic effects after pretreatment of αS during assembly. Cellular injury caused by αS-mediated perturbation of cellular redox reactions is an important proposed disease mechanism in LBD (George et al., 2009). Prior studies have shown that Mel exhibits substantial antioxidant properties (Kotler et al., 1998; Reiter et al., 1997) so that Mel has been proposed as a potential therapeutic agent in diseases in which oxidative stress is thought to be a major pathogenic factor. There is 1 opposite report that melatonin is not always neuroprotective using the rotenone model of PD (Tapias et al., 2009). However, as shown in this report, Mel dose-dependently inhibits all steps of αS assembly process. Moreover, cell culture experiments with primary neurons suggested that Mel-treated αS assemblies might be less toxic than intact αS assemblies. Thus, it may be reasonable to speculate that Mel could delay the development of LBD, not only through scavenging reactive oxygen species, but also through directly inhibiting the assembly of αS in the brain.

The concentrations of Mel are in the low nanomolar range in the blood of human. As far as cerebrospinal fluid (CSF) is concerned, peak Mel concentrations ranged from 94 to 355 pm in human (Bruce et al., 1991; Reiter, 1991). The effective concentrations of Mel for αS assembly in our experiment may be somewhat higher compared with physiological levels of Mel in the brain. However, Mel exhibited antiassembly effects at substoichiometric concentration in all steps of αS assembly process, especially oligomerization. As Mel readily crosses the blood-brain barrier, Mel may exhibit antiassembly activities in vivo when administered in high doses and for a long time.

In conclusion, our demonstration here of the potent inhibitory effects of Mel on αS assembly, coupled with previously reported redox-based protective and ameliorative effects of Mel, suggest that Mel is worthy of consideration as a therapeutic agent for LBD.

Disclosure statement

The authors disclose no conflicts of interest.

Acknowledgements

We acknowledge the support of a grant for the Knowledge Cluster Initiative (High-Tech Sensing and Knowledge Handling Technology [Brain Technology]) (MY), a grant to the Amyloidosis Research Committee from the Ministry of Health, Labor, and Welfare, Japan (MY and KO), Kanae Foundation for the Promotion of Medical Science (KO), Alumni Association of the Department of Medicine at Showa University (KO), and Nagao Memorial fund (KO). Support from the Jim Easton Consortium for Alzheimer's Drug Discovery and Biomarkers at UCLA (DBT) is also acknowledged.

Appendix A. Supplementary data

Supplementary data associated with this article can be found, in the online version, at doi:10.1016/j.neurobiolaging.2011.10.015.

References

Abe, K., Saito, H., 1998. Amyloid β protein inhibits cellular MTT reduction not by suppression of mitochondrial succinate dehydrogenase but by acceleration of MTT formazan exocytosis in cultured rat cortical astrocytes. Neurosci. Res. 31, 295–305.

Apetri, M.M., Maiti, N.C., Zagorski, M.G., Carey, P.R., Anderson, V.E., 2006. Secondary structure of α-synuclein oligomers: characterization by raman and atomic force microscopy. J. Mol. Biol. 355, 63–71.

Baba, M., Nakajo, S., Tu, P.H., Tomita, T., Nakaya, K., Lee, V.M., Trojanowski, J.Q., Iwatsubo, T., 1998. Aggregation of α-synuclein in Lewy bodies of sporadic Parkinson's disease and dementia with Lewy bodies. Am. J. Pathol. 152, 879–884.

Barrachina, M., Domínguez, I., Ambrosio, S., Secades, J., Lozano, R., Ferrer, I., 2003. Neuroprotective effect of citicoline in 6-hydroxydopamine-lesioned rats and in 6-hydroxydopamine-treated SH-SY5Y human neuroblastoma cells. J. Neurol. Sci. 215, 105–110.

Bartels, T., Choi, J.G., Selkoe, D.J., 2011. α-Synuclein occurs physiologically as a helically folded tetramer that resists aggregation. Nature 477, 107–110.

Bitan, G., Lomakin, A., Teplow, D.B., 2001. Amyloid β-protein oligomerization: prenucleation interactions revealed by photo-induced cross-linking of unmodified proteins. J. Biol. Chem. 276, 35176–35184.

Bitan, G., Teplow, D.B., 2004. Rapid photochemical cross-linking—a new tool for studies of metastable, amyloidogenic protein assemblies. Acc. Chem. Res. 37, 357–364.

Bruce, J., Tamarkin, L., Riedel, C., Markey, S., Oldfield, E., 1991. Sequential cerebrospinal fluid and plasma sampling in humans: 24-hour melatonin measurements in normal subjects and after peripheral sympathectomy. J. Clin. Endocrinol. Metab. 72, 819–823.

Caughey, B., Lansbury, P.T., 2003. Protofibrils, pores, fibrils, and neurodegeneration: separating the responsible protein aggregates from the innocent bystanders. Annu. Rev. Neurosci. 26, 267–298.

Conway, K.A., Harper, J.D., Lansbury, P.T., 1998. Accelerated in vitro fibril formation by a mutant α-synuclein linked to early-onset Parkinson disease. Nat. Med. 4, 1318–1320.

Conway, K.A., Harper, J.D., Lansbury, P.T., Jr., 2000. Fibrils formed in vitro from α-synuclein and two mutant forms linked to Parkinson's disease are typical amyloid. Biochemistry 39, 2552–2563.

Conway, K.A., Rochet, J.C., Bieganski, R.M., Lansbury, P.T., Jr., 2001. Kinetic stabilization of the α-synuclein protofibril by a dopamine-α-synuclein adduct. Science 294, 1346–1349.

El-Agnaf, O.M., Salem, S.A., Paleologou, K.E., Curran, M.D., Gibson, M.J., Court, J.A., Schlossmacher, M.G., Allsop, D., 2006. Detection of oligomeric forms of α-synuclein protein in human plasma as a potential biomarker for Parkinson's disease. FASEB J. 20, 419–425.

Evans, K.C., Berger, E.P., Cho, C.G., Weisgraber, K.H., Lansbury, P.T., Jr., 1995. Apolipoprotein E is a kinetic but not a thermodynamic inhibitor of amyloid formation: implications for the pathogenesis and treatment of Alzheimer disease. Proc. Natl. Acad. Sci. U. S. A. 92, 763–767.

Fancy, D.A., Kodadek, T., 1999. Chemistry for the analysis of protein–protein interactions: rapid and efficient cross-linking triggered by long wavelength light. Proc. Natl. Acad. Sci. U. S. A. 96, 6020–6024.

Feany, M.B., Bender, W.W., 2000. A Drosophila model of Parkinson's disease. Nature 404, 394–398.

Forno, L.S., 1996. Neuropathology of Parkinson's disease. J. Neuropathol. Exp. Neurol. 55, 259–272.

Gai, W.P., Power, J.H., Blumbergs, P.C., Blessing, W.W., 1998. Multiple-system atrophy: a new α-synuclein disease? Lancet 352, 547–548.

George, J.L., Mok, S., Moses, D., Wilkins, S., Bush, A.I., Cherny, R.A., Finkelstein, D.I., 2009. Targeting the progression of Parkinson's disease. Curr. Neuropharmacol. 7, 9–36.

Giasson, B.I., Duda, J.E., Quinn, S.M., Zhang, B., Trojanowski, J.Q., Lee, V.M., 2002. Neuronal α-synucleinopathy with severe movement disorder in mice expressing A53T human α-synuclein. Neuron 34, 521–533.

Gilman, S., Low, P.A., Quinn, N., Albanese, A., Ben-Shlomo, Y., Fowler, C.J., Kaufmann, H., Klockgether, T., Lang, A.E., Lantos, P.L., Litvan, I., Mathias, C.J., Oliver, E., Robertson, D., Schatz, I., Wenning, G.K., 1999. Consensus statement on the diagnosis of multiple system atrophy. J. Neurol. Sci. 163, 94–98.

Goedert, M., 2001. Parkinson's disease and other α-synucleinopathies. Clin. Chem. Lab. Med. 39, 308–312.

Goto, K., Mochizuki, H., Hattori, T., Nakamura, N., Mizuno, Y., 1997. Neurotoxic effects of papaverine, tetrahydropapaverine and dimethoxyphenylethylamine on dopaminergic neurons in ventral mesencephalic-striatal co-culture. Brain Res. 754, 260–268.

Ishido, M., 2007. Melatonin inhibits maneb-induced aggregation of α-synuclein in rat pheochromocytoma cells. J. Pineal Res. 42, 125–130.

Kotler, M., Rodríguez, C., Sáinz, R.M., Antolín, I., Menéndez-Peláez, A., 1998. Melatonin increases gene expression for antioxidant enzymes in rat brain cortex. J. Pineal Res. 24, 83–89.

Lashuel, H.A., Petre, B.M., Wall, J., Simon, M., Nowak, R.J., Walz, T., Lansbury, P.T., Jr., 2002. α-synuclein, especially the Parkinson's disease-associated mutants, forms pore-like annular and tubular protofibrils. J. Mol. Biol. 322, 1089–1102.

Lee, M.K., Stirling, W., Xu, Y., Xu, X., Qui, D., Mandir, A.S., Dawson, T.M., Copeland, N.G., Jenkins, N.A., Price, D.L., 2002. Human alpha-synuclein-harboring familial Parkinson's disease-linked Ala-53 –> Thr mutation causes neurodegenerative disease with alpha-synuclein aggregation in transgenic mice. Proc. Natl. Acad. Sci. U. S. A. 99, 8968–8973.

LeVine, H., 3rd, 1993. Thioflavine T interaction with synthetic Alzheimer's disease β-amyloid peptides: detection of amyloid aggregation in solution. Protein Sci. 2, 404–410.

LeVine, H., 3rd, 1999. Quantification of β-sheet amyloid fibril structures with thioflavin T. Methods Enzymol. 309, 274–284.

Li, H.T., Lin, X.J., Xie, Y.Y., Hu, H.Y., 2006. The early events of α-synuclein oligomerization revealed by photo-induced cross-linking. Protein Pept. Lett. 13, 385–390.

Li, J., Zhu, M., Rajamani, S., Uversky, V.N., Fink, A.L., 2004. Rifampicin inhibits α-synuclein fibrillation and disaggregates fibrils. Chem. Biol. 11, 1513–1521.

Lin, A.M., Fang, S.F., Chao, P.L., Yang, C.H., 2007. Melatonin attenuates arsenite-induced apoptosis in rat brain: involvement of mitochondrial and endoplasmic reticulum pathways and aggregation of α-synuclein. J. Pineal Res. 43, 163–171.

López-Burillo, S., Tan, D.X., Mayo, J.C., Sainz, R.M., Manchester, L.C., Reiter, R.J., 2003. Melatonin, xanthurenic acid, resveratrol, EGCG, vitamin C and α-lipoic acid differentially reduce oxidative DNA damage induced by Fenton reagents: a study of their individual and synergistic actions. J. Pineal Res. 34, 269–277.

Matsubara, E., Bryant-Thomas, T., Pacheco Quinto, J., Henry, T.L., Poeggeler, B., Herbert, D., Cruz-Sanchez, F., Chyan, Y.J., Smith, M.A., Perry, G., Shoji, M., Abe, K., Leone, A., Grundke-Ikbal, I., Wilson, G.L., Ghiso, J., Williams, C., Refolo, L.M., Pappolla, M.A., Chain, D.G., Neria, E., 2003. Melatonin increases survival and inhibits oxidative and amyloid pathology in a transgenic model of Alzheimer's disease. J. Neurochem. 85, 1101–1108.

McKeith, I.G., Dickson, D.W., Lowe, J., Emre, M., O'Brien, J.T., Feldman, H., Cummings, J., Duda, J.E., Lippa, C., Perry, E.K., Aarsland, D., Arai, H., Ballard, C.G., Boeve, B., Burn, D.J., Costa, D., Del Ser, T., Dubois, B., Galasko, D., Gauthier, S., Goetz, C.G., Gomez-Tortosa, E., Halliday, G., Hansen, L.A., Hardy, J., Iwatsubo, T., Kalaria, R.N., Kaufer, D., Kenny, R.A., Korczyn, A., Kosaka, K., Lee, V.M., Lees, A., Litvan, I., Londos, E., Lopez, O.L., Minoshima, S., Mizuno, Y., Molina, J.A., Mukaetova-Ladinska, E.B., Pasquier, F., Perry, R.H., Schulz, J.B., Trojanowski, J.Q., Yamada, M., Consortium on DLB, 2005. Diagnosis and management of dementia with Lewy bodies: third report of the DLB Consortium. Neurology 65, 1863–1872.

Mochizuki, H., Nakamura, N., Nishi, K., Mizuno, Y., 1994. Apoptosis is induced by 1-methyl-4-phenylpyridinium ion (MPP+) in ventral mesencephalic-striatal co-culture in rat. Neurosci. Lett. 170, 191–194.

Naiki, H., Nakakuki, K., 1996. First-order kinetic model of Alzheimer's β-amyloid fibril extension in vitro. Lab. Invest. 74, 374–383.

Nobre-Júnior, H.V., Oliveira, R.A., Maia, F.D., Nogueira, M.A., de Moraes, M.O., Bandeira, M.A., Andrade, G.M., Viana, G.S., 2009. Neuroprotective effects of chalcones from Myracrodruon urundeuva on 6-hydroxydopamine-induced cytotoxicity in rat mesencephalic cells. Neurochem. Res. 34, 1066–1075.

Ono, K., Hirohata, M., Yamada, M., 2007. Anti-fibrillogenic and fibril-destabilizing activities of anti-Parkinsonian agents for α-synuclein fibrils in vitro. J. Neurosci. Res. 85, 1547–1557.

Ono, K., Yamada, M., 2006. Antioxidant compounds have potent anti-fibrillogenic and fibril-destabilizing effects for α-synuclein fibrils in vitro. J. Neurochem. 97, 105–115.

Outeiro, T.F., Putcha, P., Tetzlaff, J.E., Spoelgen, R., Koker, M., Carvalho, F., Hyman, B.T., McLean, P.J., 2008. Formation of toxic oligomeric α-synuclein species in living cells. PLoS One 3, e1867.

Paleologou, K.E., Kragh, C.L., Mann, D.M., Salem, S.A., Al-Shami, R., Allsop, D., Hassan, A.H., Jensen, P.H., El-Agnaf, O.M., 2009. Detection of elevated levels of soluble α-synuclein oligomers in post-mortem brain extracts from patients with dementia with Lewy bodies. Brain 132, 1093–1101.

Pappolla, M., Bozner, P., Soto, C., Shao, H., Robakis, N.K., Zagorski, M., Frangione, B., Ghiso, J., 1998. Inhibition of Alzheimer β-fibrillogenesis by melatonin. J. Biol. Chem. 273, 7185–7188.

Pévet, P., Agez, L., Bothorel, B., Saboureau, M., Gauer, F., Laurent, V., Masson-Pévet, M., 2006. Melatonin in the multi-oscillatory mammalian circadian world. Chronobiol. Int. 23, 39–51.

Poeggeler, B., Miravalle, L., Zagorski, M.G., Wisniewski, T., Chyan, Y.J., Zhang, Y., Shao, H., Bryant-Thomas, T., Vidal, R., Frangione, B., Ghiso, J., Pappolla, M.A., 2001. Melatonin reverses the profibrillogenic activity of apolipoprotein E4 on the Alzheimer amyloid Aβ peptide. Biochemistry 40, 14995–15001.

Pountney, D.L., Lowe, R., Quilty, M., Vickers, J.C., Voelcker, N.H., Gai, W.P., 2004. Annular α-synuclein species from purified multiple system atrophy inclusions. J. Neurochem. 90, 502–512.

Reiter, R., Tang, L., Garcia, J.J., Muñoz-Hoyos, A., 1997. Pharmacological actions of melatonin in oxygen radical pathophysiology. Life Sci. 60, 2255–2271.

Reiter, R.J., 1991. Pineal melatonin: cell biology of its synthesis and of its physiological interactions. Endocr. Rev. 12, 151–180.

Shen, Y.X., Wei, W., Xu, S.Y., 2002a. Protective effects of melatonin on cortico-hippocampal neurotoxicity induced by amyloid β-peptide 25–35. Acta Pharmacol. Sin. 23, 71–76.

Shen, Y.X., Xu, S.Y., Wei, W., Sun, X.X., Liu, L.H., Yang, J., Dong, C., 2002b. The protective effects of melatonin from oxidative damage induced by amyloid β-peptide 25–35 in middle-aged rats. J. Pineal Res. 32, 85–89.

Shen, Y.X., Xu, S.Y., Wei, W., Wang, X.L., Wang, H., Sun, X., 2002c. Melatonin blocks rat hippocampal neuronal apoptosis induced by amyloid β-peptide 25–35. J. Pineal Res. 32, 163–167.

Spillantini, M.G., Crowther, R.A., Jakes, R., Cairns, N.J., Lantos, P.L., Goedert, M., 1998. Filamentous α-synuclein inclusions link multiple system atrophy with Parkinson's disease and dementia with Lewy bodies. Neurosci. Lett. 251, 205–208.

Srinivasan, V., Pandi-Perumal, S.R., Maestroni, G.J., Esquifino, A.I., Hardeland, R., Cardinali, D.P., 2005. Role of melatonin in neurodegenerative diseases. Neurotox. Res. 7, 293–318.

Storch, A., Hwang, Y.I., Gearhart, D.A., Beach, J.W., Neafsey, E.J., Collins, M.A., Schwarz, J., 2004. Dopamine transporter-mediated cytotoxicity of β-carbolinium derivatives related to Parkinson's disease: relationship to transporter-dependent uptake. J. Neurochem. 89, 685–694.

Taniguchi, S., Suzuki, N., Masuda, M., Hisanaga, S., Iwatsubo, T., Goedert, M., Hasegawa, M., 2005. Inhibition of heparin-induced tau filament formation by phenothiazines, polyphenols, and porphyrins. J. Biol. Chem. 280, 7614–7623.

Tapias, V., Cannon, J.R., Greenamyre, J.T., 2009. Melatonin treatment potentiates neurodegeneration in a rat rotenone Parkinson's disease model. J. Neurosci. Res. 88, 420–427.

Tsigelny, I.F., Crews, L., Desplats, P., Shaked, G.M., Sharikov, Y., Mizuno, H., Spencer, B., Rockenstein, E., Trejo, M., Platoshyn, O., Yuan, J.X., Masliah, E., 2008. Mechanisms of hybrid oligomer formation in the pathogenesis of combined Alzheimer's and Parkinson's diseases. PLoS One 3, e3135.

Volles, M.J., Lansbury, P.T., Jr., 2003. Zeroing in on the pathogenic form of α-synuclein and its mechanism of neurotoxicity in Parkinson's disease. Biochemistry 42, 7871–7878.

Volles, M.J., Lee, S.J., Rochet, J.C., Shtilerman, M.D., Ding, T.T., Kessler, J.C., Lansbury, P.T., Jr., 2001. Vesicle permeabilization by protofibrillar α-synuclein: implications for the pathogenesis and treatment of Parkinson's disease. Biochemistry 40, 7812–7819.

Wood, S.J., Wypych, J., Steavenson, S., Louis, J.C., Citron, M., Biere, A.L., 1999. α-synuclein fibrillogenesis is nucleation-dependent. Implications for the pathogenesis of Parkinson's disease. J. Biol. Chem. 274, 19509–19512.

Xu, J., Kao, S.Y., Lee, F.J., Song, W., Jin, L.W., Yankner, B.A., 2002. Dopamine-dependent neurotoxicity of α-synuclein: a mechanism for selective neurodegeneration in Parkinson disease. Nat. Med. 8, 600–606.

Yazawa, I., Giasson, B.I., Sasaki, R., Zhang, B., Joyce, S., Uryu, K., Trojanowski, J.Q., Lee, V.M., 2005. Mouse model of multiple system atrophy α-synuclein expression in oligodendrocytes causes glial and neuronal degeneration. Neuron 45, 847–859.

Zhu, M., Rajamani, S., Kaylor, J., Han, S., Zhou, F., Fink, A.L., 2004. The flavonoid baicalein inhibits fibrillation of α-synuclein and disaggregates existing fibrils. J. Biol. Chem. 279, 26846–26857.

doi:10.1093/brain/awr348 Brain 2012: 135; 833–846 | 833

BRAIN
A JOURNAL OF NEUROLOGY

Non-human primate model of amyotrophic lateral sclerosis with cytoplasmic mislocalization of TDP-43

Azusa Uchida,[1] Hiroki Sasaguri,[1] Nobuyuki Kimura,[2] Mio Tajiri,[1] Takuya Ohkubo,[1] Fumiko Ono,[3] Fumika Sakaue,[1] Kazuaki Kanai,[4] Takashi Hirai,[5] Tatsuhiko Sano,[1] Kazumoto Shibuya,[4] Masaki Kobayashi,[1] Mariko Yamamoto,[1] Shigefumi Yokota,[1] Takayuki Kubodera,[1] Masaki Tomori,[5] Kyohei Sakaki,[5] Mitsuhiro Enomoto,[5] Yukihiko Hirai,[6] Jiro Kumagai,[7] Yasuhiro Yasutomi,[2] Hideki Mochizuki,[8] Satoshi Kuwabara,[4] Toshiki Uchihara,[9] Hidehiro Mizusawa[1] and Takanori Yokota[1]

1 Department of Neurology and Neurological Science, Graduate School of Medicine, Tokyo Medical and Dental University, Tokyo 113-8519, Japan
2 Tsukuba Primate Research Centre, National Institute of Biomedical Innovation, Tsukuba 305-0843, Japan
3 Corporation for Production and Research of Laboratory Primates, Tsukuba 305-0843, Japan
4 Department of Neurology, Graduate School of Medicine, Chiba University, Chiba 260-8670, Japan
5 Department of Orthopaedic Surgery, Graduate School of Medicine, Tokyo Medical and Dental University, Tokyo 113-8519, Japan
6 Department of Biochemistry and Molecular Biology, Nippon Medical School, Tokyo 113-8602, Japan
7 Department of Pathology, Graduate School of Medicine, Tokyo Medical and Dental University, Tokyo 113-8519, Japan
8 Department of Neurology, Kitasato University School of Medicine, Kanagawa 228-8555, Japan
9 Laboratory of Structural Neuropathology, Tokyo Metropolitan Institute of Medical Science, Tokyo 156-8506, Japan

Correspondence to: Takanori Yokota,
Department of Neurology and Neurological Science,
Graduate School of Medicine,
Tokyo Medical and Dental University,
Bunkyo-ku, Tokyo 113-8519,
Japan
E-mail: tak-yokota.nuro@tmd.ac.jp

Amyotrophic lateral sclerosis is a fatal neurodegenerative disease characterized by progressive motoneuron loss. Redistribution of transactive response deoxyribonucleic acid-binding protein 43 from the nucleus to the cytoplasm and the presence of cystatin C-positive Bunina bodies are considered pathological hallmarks of amyotrophic lateral sclerosis, but their significance has not been fully elucidated. Since all reported rodent transgenic models using wild-type transactive response deoxyribonucleic acid-binding protein 43 failed to recapitulate these features, we expected a species difference and aimed to make a non-human primate model of amyotrophic lateral sclerosis. We overexpressed wild-type human transactive response deoxyribonucleic acid-binding protein 43 in spinal cords of cynomolgus monkeys and rats by injecting adeno-associated virus vector into the cervical cord, and examined the phenotype using behavioural, electrophysiological, neuropathological and biochemical analyses. These monkeys developed progressive motor weakness and muscle atrophy with fasciculation in distal hand muscles first. They also showed regional cytoplasmic transactive response deoxyribonucleic acid-binding protein 43 mislocalization with loss of nuclear transactive response deoxyribonucleic acid-binding protein 43 staining in the lateral nuclear group of spinal cord innervating distal hand muscles and cystatin C-positive cytoplasmic aggregates, reminiscent of the spinal cord pathology of patients with amyotrophic lateral sclerosis. Transactive response deoxyribonucleic acid-binding protein 43 mislocalization was

Received July 27, 2011. Revised October 26, 2011. Accepted November 14, 2011. Advance Access publication January 17, 2012

an early or presymptomatic event and was later associated with neuron loss. These findings suggest that the transactive response deoxyribonucleic acid-binding protein 43 mislocalization leads to α-motoneuron degeneration. Furthermore, truncation of transactive response deoxyribonucleic acid-binding protein 43 was not a prerequisite for motoneuronal degeneration, and phosphorylation of transactive response deoxyribonucleic acid-binding protein 43 occurred after degeneration had begun. In contrast, similarly prepared rat models expressed transactive response deoxyribonucleic acid-binding protein 43 only in the nucleus of motoneurons. There is thus a species difference in transactive response deoxyribonucleic acid-binding protein 43 pathology, and our monkey model recapitulates amyotrophic lateral sclerosis pathology to a greater extent than rodent models, providing a valuable tool for studying the pathogenesis of sporadic amyotrophic lateral sclerosis.

Keywords: TDP-43; Bunina bodies; cystatin C; cynomolgus monkeys; amyotrophic lateral sclerosis

Abbreviations: AAV = adeno-associated virus; ALS = amyotrophic lateral sclerosis; FTLD = frontotemporal lobar degeneration; HEK = human embryonic kidney; TDP-43 = transactive response DNA-binding protein 43

Introduction

Amyotrophic lateral sclerosis (ALS), also known as Lou Gehrig's disease, is an incurable progressive neurodegenerative disease characterized by muscle weakness and atrophy resulting from the combined loss of upper and lower motoneurons. Most cases of ALS are sporadic, and only 10% of ALS cases are of a familial form. Protein aggregates are one histopathological characteristic of ALS. A breakthrough in understanding ALS pathogenesis was the discovery of the 43-kDa transactive response DNA-binding protein (TDP-43), which was recently identified as the major component of the protein aggregates and of the insoluble fraction in the brains of patients with sporadic ALS and frontotemporal lobar degeneration (FTLD) (Arai *et al.*, 2006; Neumann *et al.*, 2006). TDP-43 is now expected to play an essential role in the pathogenesis of sporadic ALS, possibly equivalent to that of tau and beta amyloid in Alzheimer's disease or α-synuclein in Parkinson's disease.

Human TDP-43 is a highly conserved and ubiquitously expressed 414 amino acid nuclear protein that binds to both DNA and RNA (Ou *et al.*, 1995; Buratti *et al.*, 2001). In normal settings, TDP-43 is a primarily nuclear protein that functions in transcription regulation, alternative splicing and RNA stabilization (Buratti *et al.*, 2008), as well as in microRNA metabolism (Buratti *et al.*, 2010). Pathological TDP-43 can be abnormally truncated, phosphorylated and ubiquitinated, and most TDP-43 is mislocalized from the nucleus to the cytoplasm or neurites (Arai *et al.*, 2006; Neumann *et al.*, 2006). Of note, almost all neurons with cytoplasmic TDP-43 accumulations show a dramatic depletion of normal nuclear TDP-43. Thus, both gain and loss of functions are potential disease mechanisms, either due to the loss of normal nuclear TDP-43 expression, or cytoplasmic mislocalization (Arai *et al.*, 2006; Neumann *et al.*, 2006; Cairns *et al.*, 2007). Therefore, cytoplasmic TDP-43 mislocalization with loss of its nuclear staining is a key feature found in the majority of patients' brains and spinal cords (Arai *et al.*, 2006; Neumann *et al.*, 2006).

TDP-43 strictly regulates its messenger RNA levels by directly binding to an intron in the 3′-untranslated region of its own transcript and enhancing its splicing (Ayala *et al.*, 2010; Polymenidou *et al.*, 2011), however, the expression level of TDP-43 can be upregulated ~1.5-fold (Mishra *et al.*, 2007; Gitcho *et al.*, 2009) in FTLD/ALS. Moreover, mutations in the *TDP-43* gene are associated with familial ALS (Kabashi *et al.*, 2008; Yokoseki *et al.*, 2008), in which TDP-43 is also frequently mislocalized within motoneurons of the spinal cord. These reports support the hypothesis that mislocalization of this protein plays a central role in the disease pathogenesis. The rodent, *Drosophila*, *Ceanorhabditis elegans* and zebrafish models with overexpressed mutant as well as wild-type TDP-43 show severe motor symptoms and wild-type TDP-43 localizes exclusively or primarily to nuclei (Ash *et al.*, 2010; Hanson *et al.*, 2010; Kabashi *et al.*, 2010; Li *et al.*, 2010; Shan *et al.*, 2010; Voigt *et al.*, 2010; Wils *et al.*, 2010; Xu *et al.*, 2010; Swarup *et al.*, 2011), although mutant TDP-43 is more likely to accumulate in the cytoplasm (Swarup *et al.*, 2011). The results of the rodent models suggested that overexpressed nuclear wild-type TDP-43 is toxic, but provide little insight for the significance of mislocalized wild-type TDP-43. Even in mouse models that overexpress wild-type TDP-43 with mutated nuclear localization signals, total human and mouse nuclear TDP-43 was not reduced (Igaz *et al.*, 2011) when compared with that in littermate wild-type controls. Together, these reported mouse models might have a different TDP-43 pathology from that found in patients with ALS. Expecting that a primate model of ALS might more closely reflect the TDP-43 pathology in human patients with ALS, we overexpressed human wild-type TDP-43 in the spinal motoneurons of a non-human primate, the cynomolgus monkey, using an adeno-associated virus (AAV) 1 vector.

Materials and methods

Human subjects

Neurologists clinically diagnosed ALS with the aid of electrophysiological examinations. The clinical diagnosis of definite ALS was based on El Escorial (Brooks *et al.*, 2000) and electrodiagnostic (De Carvalho *et al.*, 2008) criteria and confirmed by neuropathological examination in accordance with published guidelines (Piao *et al.*, 2003).

The patient study protocol was approved by the institutional clinical study committee at Tokyo Medical and Dental University (No. 799). Consent forms for autopsy were obtained from legal representatives of all patients in accordance with the guidelines of the institutional review boards.

Animals

Ten male adult cynomolgus monkeys (*Macaca fascicularis*; 3–7 years old, 3.28–5.10 kg) were bred and treated at Tsukuba Primate Research Centre. The number of monkeys and concentrations of viral stocks were as follows: one monkey was injected with high-dose Flag-TDP-43 AAV1 [1×10^{13} viral genomes (vg)/ml]; six monkeys were injected with low-dose Flag-TDP-43 AAV1 (3×10^{12} vg/ml); three monkeys were injected with low-dose mock AAV1 (3×10^{12} vg/ml) as a negative control. Three monkeys injected with low-dose TDP-43 AAV1 were pathologically examined in the early stage, 3–5 days after the onset of motor symptoms and the other three monkeys were examined in the late stage, 4–7 weeks after injection.

Eleven adult male Fisher rats (10 weeks old, Sankyo-lab) were used. The number of rats and concentrations of viral stocks were as follows: eight rats were injected with low-dose Flag-TDP-43 AAV1 (3×10^{12} vg/ml) and three rats were injected with low-dose control AAV1 (3×10^{12} vg/ml) as a negative control. Three rats injected with TDP-43 AAV1 were pathologically examined in the early stage, 1–2 weeks after injection, and the others were examined in the late stage, 4–9 weeks after injection.

All animal experiments were conducted according to the U.S. National Institutes of Health Guide for the Care and Use of Laboratory Animals, and the Guidelines for the Animal Care and Management of the Tsukuba Primate Research Center and Tokyo Medical and Dental University.

Constructs

Human wild-type TDP-43 was purchased from Invitrogen. The TDP-43 and Flag-TDP-43 fragments were generated by polymerase chain reaction using the following primer pairs: 5′-CCGCTCGAGGCCACCATG GATTAC AAGGATGACGACGATAAGTCTGAATATATTCGGGTAA CCGG-3′ and 5′-CCGCTCGAGCTACATTCCCCAG CCAGAAG ACTTA-3′ for TDP-43, and 5′-CCGCTCGAGGCCACCATGGATTACA AGGATGACGACGAT AAGTCTGAATATATTCGGGTAACCGG-3′ and 5′-CCGCTCGAGCTACATTCCCCAGCCAGAAGACTTA-3′ for Flag-TDP-43, which contained XhoI digestion sites at the 3′- and 5′-ends. The Flag-TDP-43 complementary DNA was subcloned into an expression cassette flanked with AAV2 inverted terminal repeats (Stratagene). The cytomegalovirus (CMV) promoter was used to drive expression.

Adeno-associated virus preparations

Human embryonic kidney (HEK) 293 cells at ~70% confluence were transfected with the AAV1 packaging plasmid pRep2/Cap9 (gift from Dr James M. Wilson, University of Pennsylvania) and adenovirus helper plasmid (Stratagene) at a ratio of 1:1:1. At 6 h after transfection, the culture medium was replaced with fresh medium, and the cells were incubated for 48 h. The cells were then harvested from the culture dishes and pelleted by centrifugation, resuspended in phosphate-buffered saline and subjected to three rounds of freeze–thawing. Cell debris was then pelleted by centrifugation at 1200*g* for 15 min. AAV vectors were purified using ammonium sulphate precipitation and iodixanol (Axis-Shield) continuous gradient centrifugation.

Size-exclusion chromatography was performed using an AKTA Explorer 100 HPLC system (GE Healthcare) equipped with a 2-ml sample loop. A Superdex 200 10/300 GL column (GE Healthcare) was equilibrated with MHA buffer (3.3 mM MES, 3.3 mM HEPES, 3.3 mM NaOAc, 50 mM NaCl, pH 6.5). The vector-containing fractions were loaded onto the column at a flow rate of 0.5 ml/min, and the eluate was collected as 0.5 ml fractions over the duration of one column volume (23 ml). AAV peak fractions were identified by 280/260 nm absorbance and real-time quantitative polymerase chain reaction using vector-specific primers. The purified AAVs were then concentrated further by using Amico Ultra-4 tubes (Ultracel-30k, Millipore) to a final concentration of 1×10^{13} genome copies/ml, as determined by real-time quantitative polymerase chain reaction.

The genome copy number was calculated by TaqMan® PCR (Applied Biosystems). The vectors were treated with Benzonase® and digested with proteinase K (Wako Pure Chemical Industries) for 1 h and purified by phenol–chloroform extraction. The TaqMan® primers and probe were designed as follows: forward primer: 5′-CAGGCTGGT CCAACTCCTA-3′, reverse primer: 5′-GCAGTGGTTCACGCCTGTAA-3′, and probe: 5′-TACCCACCTTGGCCTC-3′. The designed TaqMan® PCR fragment was located in the human growth hormone polyadenylation site in the vector.

Successful viral assembly of control AAV and transgene expression were confirmed by immunoblot analysis using HEK 293 cells infected with AAV (Supplementary Fig. 1), as described below.

HEK-293 cells were cultured in Dulbecco's modified Eagle's medium containing 10% foetal bovine serum with 1% penicillin/streptomycin. The cells in 12-well plates were infected by Flag-TDP-43 AAV1 (5×10^{10} vg/ml). At 48 h after infection, cells were harvested by gentle scraping in lysis buffer [20 mM Tris–HCl, 150 mM NaCl, 1% NP-40, 0.1% deoxicolate, 1% sodium dodecyl sulphate, 1 mM EDTA, 1 mM EGTA, 10 mM β-glycerophosphate, 5 mM NaF and Complete protease inhibitor cocktail (Roche Diagnostics)]. Equal amounts of total cellular protein were mixed with 5× Laemmli sample buffer, denatured at 95°C for 5 min, and separated with 10% sodium dodecyl sulphate polyacrylamide gel electrophoresis. The proteins were transferred to PVDF membranes. After blocking with 3% gelatin (Wako Pure Chemical Industry) in Tris-buffered saline or 5% skimmed milk (Wako Pure Chemical Industry) in Tris-buffered saline-Triton X-100, the membranes were incubated overnight with the following primary antibodies: anti-M2 (1:2000); anti-pan-TDP-43 (1:2000); and anti-VP1, VP2 and VP3 of AAV (1:1000). After incubation with an appropriate horseradish peroxidase-conjugated secondary antibody (Santa Cruz Biotechnology), labelling was detected with the ECL Plus™ Chemiluminescent Detection System (GE Healthcare) or SuperSignal (Thermo Scientific).

Stereotaxic injection of adeno-associated viral vectors

All surgical operations were performed under general anaesthesia. Ketamine hydrochloride (Ketalar, Sankyo) was intramuscularly administered at a dose of 5 mg/kg as a pre-anaesthetic agent, and general anaesthesia was maintained with isoflurane (Forane, Abbott) and oxygen after tracheal intubation. The monkeys were positioned in a stereotaxic frame. After a bilateral laminectomy and opening the dura in the midline at C5–6, AAV vectors were stereotaxically injected into the side ipsilateral to the dominant hand. The injection site was determined and depth of needle insertion was calculated from the preoperatively taken MRI of cervical spinal cord. AAV stock (5 µl) was injected through a 31-gauge needle connected to a 10-µl Hamilton microsyringe in 2 min. The needle remained in place for 10 min and was removed slowly. The dura and skin were sutured and monkeys returned to their individual cages. The monkeys received 0.5 mg/kg butorphanol tartrate (Stadol, Bristol-Myers Squibb) intramuscularly for 3 days to alleviate any postoperative pain.

The rats were anaesthetized with an intraperitoneally administered cocktail of 1.5 ml chloral hydrate (70 mg/ml, Wako Pure Chemical Industry) and 0.1 ml ketamine hydrochloride (70 mg/ml) at a dose of 6 ml/kg. A left side hemi-laminectomy was performed from C4 to C6. On the left side of the C6 segment, 1.5 µl of viral stock was manually injected through sharpened microcapillary glass (PN-30 puller, Narishige) connected via silicone to a 10-µl Hamilton microsyringe at a rate of 0.5 µl/min. The sharpened microcapillary glass remained in place for 3 min and was removed slowly. The skin was sutured, the rats placed on a heating pad until they began to recover from surgery, and then returned to their individual cages.

For detection of the AAV genome in the spinal cord, total DNA was extracted from spinal cord with homogenized buffer containing 0.5% sodium dodecyl sulphate, 10 mM Tris–HCl pH 8.0, and 10 mM EDTA pH 8.0, and polymerase chain reactions were carried out with the following primer pair: 5′-CGCTGTTTTGACCTCCATAGAA-3′ and 5′-AGGCGGTACTTACGTCACTCTTG-3′ for the cytomegalovirus β-globin intron.

Behavioural analysis

For monkeys, to evaluate weakness of the forelimb muscles on the AAV-injected side (the dominant-hand side), we performed the 'apple test'. The front fence of the cage was altered to have two holes and trays on the right and left side. A piece of apple was placed in line from back (monkey side) to front (observer side) on the left or right tray at 3, 6, 9 and 12 cm from the front fence during a session. The monkeys were trained to reach a small piece of apple on the trays through the hole. Four sessions were performed alternately for each side. We analysed how frequently a monkey used his dominant hand to pick up apples before and every week after the operations. We also carefully observed behaviour of the monkeys in daily life every day and recorded video monitoring for 30 min per week.

For rats, to evaluate weakness of the forelimb muscles, we measured grip strength using a special device (Muromachi Kiki) as previously described (Anderson, 2005).

Electrophysiological assessment

The nerve conduction study and needle EMG studies were performed under anaesthesia with a combination of 7 mg/kg ketamine hydrochloride and 1.2 mg/kg xylazine administrated intramuscularly. Nerve conduction studies were performed in the bilateral median nerves using conventional procedures and an EMG Machine (MEB-2300, Nihon-koden). The recording surface electrode was placed over the belly of the thenar eminence with a reference electrode at the metacarpophalangeal joint of the thumb, and compound muscle action potentials were elicited after the stimulation of the median nerve at the wrist. The peak-to-peak amplitudes were measured for all compound muscle action potentials. Nerve conduction studies were examined before AAV injection and every 1 or 2 weeks after. The needle EMG study was performed in the first dorsal interosseous, flexor carpi ulnaris and biceps brachii muscles using a conventional concentric needle electrode used in human studies (TECA Elite, CareFusion), 4–6 weeks after AAV injection.

Neuropathological examinations

Animals were deeply anaesthetized first with intramuscularly administered 7 mg/kg ketamine hydrochloride and then with intravenously administered 25 mg/kg pentobarbital. After confirming the absence of a blink reflex, the spinal cord and skeletal muscles were removed. For neuropathological examination, human and animal spinal cord samples were immersion fixed in 10% neutral buffered formalin, processed conventionally, embedded in paraffin, cut into 4-µm-thick sections and stained with haematoxylin and eosin. For immunostaining, sections were deparaffinized, pretreated in 0.5% periodic acid, autoclaved for 5 min at 121°C and then incubated free-floating overnight at 4°C with the following primary antibodies: M2 (1:500), anti-pan-TDP-43 (1:1000), anti-pS409/410-TDP-43 (1:500), anti-ubiquitin (1:500), anti-p62 (1:500), anti-cystatin-C (1:1000), anti-GFAP (1:500), anti-GLUT-5 (1:500) and SMI31 (1:200). Following brief washes, the sections were sequentially incubated with polymer immunocomplex (Dako)

Immunoreactive elements were visualized by treating sections with 3,3′ diaminobenzidine tetroxide (DAB-4HCl, Dojin Kagaku) with or without nickel ammonium chloride. The sections were then counterstained with haematoxylin. For double-immunostaining, the deparaffinized sections were stained with Sudan Black B to avoid autofluorescence. The free-floating sections were incubated overnight at 4°C in solutions containing the primary antibodies. The sections were then incubated with AlexaFluor 488- or 555-conjugated secondary antibodies (1:500, Invitrogen), and DAPI nuclear stain (1:500, Santa Cruz Biotechnology) for 1 h. All sections were examined using a confocal microscope (NIKON or Carl Zeiss).

Animal anterior root samples were fixed with a mixture of 2.5% glutaraldehyde in 0.1 M phosphate buffer (pH 7.4) at 4°C overnight, and then further fixed in 1% osmium tetroxide in 0.1 M phosphate buffer (pH 7.4) for 1 h. The well-fixed tissues were dehydrated in graded ethanol and embedded in Epon 812 (Poly/Bed® 812, Polyscience). The fixed roots were transversely cut into 1-µm-thick sections and stained with toluidine blue.

For counting of anterior horn neurons in the spinal cord, monkey eighth cervical segments were serially cut at 4-µm thickness, and every fifth section was stained with haematoxylin and eosin. The previous and next serial sections (that is, every fourth and sixth sections) were immunostained with anti-pan-TDP-43 or anti-Flag antibodies. The number and minimum diameters of neurons with nuclei in the lateral or medial nuclear groups in 15 sections were evaluated using the Image J software program from the U.S. National Institutes of Health.

Antibody information

We used the following primary antibodies for immunostaining and immunoblot analyses: mouse monoclonal anti-Flag (M2, Sigma); rabbit polyclonal anti-pan-TDP-43 (10782-1-AP, ProteinTech Group); rabbit polyclonal anti-C-terminal TDP-43 (12892-1-AP, ProteinTech Group); rabbit polyclonal anti-phosphorylated S409/410 TDP-43 (Cosmo Bio); rabbit polyclonal anti-ubiquitin (Dako); rabbit polyclonal anti-cystatin-C (Dako); mouse monoclonal anti-phosphorylated neurofilament (SMI31, Sternberger Monoclonals); rabbit polyclonal anti-glial fibrillary acidic protein (GFAP) (Dako); rabbit polyclonal anti-glucose transporter 5 (GLUT-5, IBL); rabbit polyclonal and mouse monoclonal anti-peripeherin (AB1530 and AB1527, Chemicon); mouse monoclonal anti-neurofilament light (N5139, Sigma) antibody; anti-p62 (GP62-C, Progen); anti-glyceraldehyde-3-phosphate dehydrogenase (GAPDH, Biodesign), and anti-AAV capsid proteins VP1, VP2 and VP3 (Progen Biotechnik).

Sequential biochemical fractionation, dephosphorylation and immunoblot analysis

Frozen frontal cortex or spinal cord (50–250 mg) was homogenized in 10 volumes of buffer A (10 mM Tris–HCl pH 7.5, containing 1 mM

EGTA, 10% sucrose and 0.8 M NaCl). After the addition of Triton X-100 at a final concentration of 1%, the homogenate was incubated for 30 min at 37°C and spun at 100 000*g* for 20 min at 20°C. The pellet was homogenized in 20 volumes of buffer A containing 1% sarkosyl, incubated for 30 min at 37°C and spun at 100 000 *g* for 20 min at 20°C. The sarkosyl-insoluble pellet was homogenized in four volumes of buffer A containing 1% CHAPS [3-[(3-cholamidopropyl)dimethylammonio]-1-propanesulphonate] and spun at 100 000*g* for 20 min. The pellet was sonicated in 0.5 volume of 8 mol/l urea buffer, cleared by centrifugation at 100 000*g* for 20 min at 20°C, and used for immunoblotting. The samples before (−) and after (+) treatment with lambda protein phosphatase (1600 U/ml, New England Biolabs) were subjected to 10% sodium dodecyl sulphate polyacrylamide gel electrophoresis. Proteins in the gel were then transferred onto a polyvinylidene difluoride (PVDF) membrane (Millipore). After blocking with 3% gelatin (Wako Pure Chemical Industries) in Tris-buffered saline (50 mM Tris–HCl pH 7.5, 150 mM NaCl), the membranes were incubated overnight with the following primary antibodies: anti-M2 (1:2000); anti-C-TDP-43 (1:1200); anti-phosphorylated S409/410 TDP-43 (1:2000); anti-p62 (1:3000) and anti-GAPDH (1:2000). After incubation with an appropriate horseradish peroxidase-conjugated secondary antibody (Santa Cruz Biotechnology), labelling was detected by a 3,3′diaminobendizene reaction intensified with nickel chloride (Metal-Enhanced DAB Substrate Kit, Thermo Scientific), the ECL Plus™ Chemiluminescent Detection System (GE Healthcare), or SuperSignal (Thermo Scientific).

Quantitative real-time polymerase chain reaction assay

Total RNA was extracted from whole-brain homogenates with Isogen (Nippon Gene). DNase-treated RNA (2.5 μg) was reverse-transcribed with SuperScript® III and random hexamers (Life Technologies). Complementary DNA was amplified by the quantitative TaqMan® system by using the Light Cycler 480 Real-Time PCR Instrument (Roche Diagnostics). The primers and probes specific for Flag-tagged human TDP-43, rat TDP-43 (NM_001011979.2) and monkey TDP-43 (XM_001102660.2) were designed. Relative Flag-human TDP-43 messenger RNA levels were calculated in comparison to endogenous rat or cynomolgus messenger RNA levels. A list of all primers and probes used in this study is provided in Supplementary Table 1.

Statistical analysis

The data obtained from independent experiments are presented as means ± SEM.

Statistical analysis of spinal neuron counts and axonal density among TDP-43-expressed monkey group in early, late stage and control monkey group by one-way ANOVA with Bonferroni's *post hoc* test. $P < 0.05$ was considered significant.

Results

Overexpressing wild-type TDP-43 in the monkey cervical cord leads to progressive motor weakness and muscle atrophy with fasciculation

AAV expressing Flag-tagged TDP-43 (Supplementary Fig. 2) was directly injected into the sixth cervical segment on the dominant-hand side of seven monkeys. All monkeys developed progressive motor weakness and muscle atrophy with marked fasciculation in the forelimb on the injected side (Fig. 1A and B, Supplementary Video 1). Two to 3 weeks after the injection, the TDP-43-expressing monkeys first showed some difficulty in taking time to pick up pieces of apple using the dominant hand on the injected side in the apple test, and changed to use the non-dominant hand (Fig. 1C). On observation by video monitoring, they could reach and grasp the ceiling fence at the onset of clumsiness of picking apples, but 1–3 weeks later could not flex the elbow joint and raise the forelimb, indicating the motor weakness had spread to the proximal muscles (Fig. 1D). In the late stage, 2–5 weeks after the onset, the dominant hand muscles became completely paralysed (Fig. 1A), and muscle weakness and atrophy had spread to the contralateral, un-injected side limb muscles (Fig. 1B and E). One of TDP-43-expressing monkeys showed respiratory failure at the end stage. The control monkeys did not show obvious motor symptoms, indicating surgical procedure or virus toxicity was minimal (Fig. 1C–E and Supplementary Video 2).

Electrophysiological findings

Electrophysiologically, in all TDP-43-expressing monkeys, the compound muscle action potential of the thenar muscle evoked by stimulation of the median nerve at the wrist progressively decreased in size with preservation of conduction velocity, and the muscle became unexcitable in the late stage (Fig. 2A). In contrast, three monkeys injected with control AAV did not show a marked change compound muscle action potential size (Fig. 2A). In TDP-43-expressing monkeys, the compound muscle action potential size on the contralateral side was not changed in the early stage (3–5 days after the onset of motor symptoms), but showed milder reduction of compound muscle action potential size in the late stage (Fig. 2B). Needle EMG revealed robust fasciculation potentials, and denervating potentials of positive sharp waves and fibrillation potentials in the late stage (Fig. 2C).

Cytoplasmic mislocalization with loss of endogenous monkey TDP-43, dystrophic neurites and cystatin C-positive granules in the cytoplasm

Neuropathologically, an anti-Flag antibody widely detected exogenous TDP-43 in neurons from the second cervical to the second thoracic segments on both sides, and was observed in almost all neurons on the injected side from the fourth to eighth cervical segments. Generally, Flag immunoreactivity was not detected in the glial cells. There was no inflammatory reaction except for in the area around the injection site. In the late stage, exogenous TDP-43 was observed in either the nucleus or cytoplasm (Fig. 3A). Pan-TDP-43 staining revealed that most motoneurons with cytoplasmic TDP-43 lost endogenous monkey TDP-43 staining (Fig. 3B), which normally localized in the nucleus (Fig. 3C). Mislocalized TDP-43 was diffusely distributed in the cytoplasm

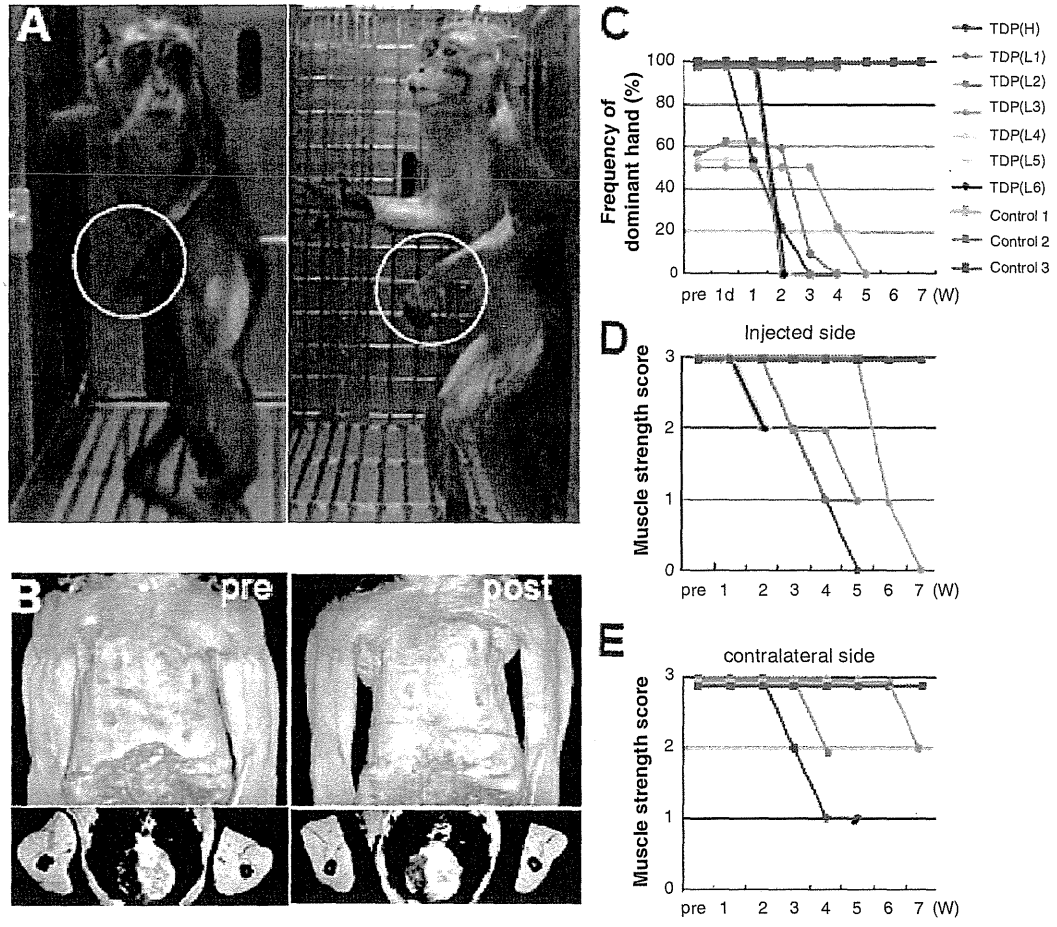

Figure 1 Overexpressing wild-type TDP-43 in the monkey cervical cord leads to progressive motor weakness and muscle atrophy. (**A**) Motor paresis of the forelimb on the injected side (encircled) in TDP-43 AAV-injected monkeys. (**B**) Constructed (*top*) and axial (*bottom*) MRI images of upper arm muscles before (pre) and 4 weeks after (post) injection, indicating a marked muscle atrophy of upper and forearms as well as hand muscles, predominantly on the injected side (left side). (**C**) Apple test. Frequency with which the dominant hand was used to pick up apples. (**D** and **E**) Behavioural analysis assessing muscle strength of forearms on the injected side (**D**) and contralateral side (**E**). A score of 3 indicates that the monkeys can hang on the ceiling fence; score of 2, they can grasp but not hang on the ceiling fence; score of 1, they can raise the forelimb but not reach ceiling fence; score of 0, they cannot raise the forelimb. Measurements that appear to end before the end of the experiment are from the three monkeys that were pathologically examined in the early stage.

and, in some neurons, granularly aggregated (Fig. 3B). Proximal and distal dystrophic neurites were occasionally observed (Fig. 3A and B). Phosphorylation of TDP-43 in the nucleus or cytoplasm was not clear in the early stage, but became obvious in the late stage (Fig. 3D). Anti-ubiquitin and anti-p62 antibodies did not show a clear abnormal signal. Astrogliosis and microgliosis were observed (Supplementary Fig. 3). A small fraction of the motoneurons expressing TDP-43 in the nucleus characteristically displayed coarse cystatin C-positive granules in the cytoplasm (Fig. 3E) in the neurons with exogenously expressed TDP-43 in the nucleus. There were no neurons with co-localized cystatin C-positive granules and TDP-43 aggregates in the cytoplasm. We also observed aberrant accumulation of phosphorylated neurofilaments (Fig. 3F) and peripherin (Supplementary Fig. 4) in the cytoplasm of spinal motoneurons, a common pathological feature in patients with ALS (Munoz *et al.*, 1988; Corbo and Hays, 1992).

Immunostaining with an anti-Flag antibody identified its nuclear or cytoplasmic immunoreactivity in some Betz cells in the precentral gyrus restricted to the forelimb area contralateral to the injection. This Flag immunoreactivity was not observed in other cortical areas (including hippocampus and frontal lobe, which are preferentially affected in patients with FTLD), thalamus, basal ganglia and white matter, or in glial cells (Supplementary Fig. 5).

Characteristic regional mislocalization of TDP-43 in motoneurons of the anterior horn similar to amyotrophic lateral sclerosis spinal cords

In the early stage, 3–5 days after the onset of hand clumsiness, TDP-43 mislocalization of diffuse staining pattern was observed in